Received: 9 November 2022 | Revised: 27 February 2023 | Accepted: 20 March 2023

DOI: 10.1111/bre.12765

Basin Research | IAS EAGE | WILEY

RESEARCH ARTICLE

Source-to-sink mass-balance analysis of an ancient wave-influenced sediment routing system: Middle Jurassic Brent Delta, Northern North Sea, offshore UK and Norway

Ikenna C. Okwara[1,2] | **Gary J. Hampson**[1] | **Alexander C. Whittaker**[1] | **Gareth G. Roberts**[1] | **Patrick W. Ball**[3]

[1]Department of Earth Science and Engineering, Imperial College London, London, UK

[2]Department of Geology, University of Nigeria, Nsukka, Nigeria

[3]Department of Geosciences, Colorado State University, Fort Collins, Colorado, USA

Correspondence
Gary J. Hampson, Department of Geology, University of Nigeria, Nsukka, Nigeria.
Email: g.j.hampson@imperial.ac.uk

Funding information
Petroleum Technology Development Fund, Grant/Award Number: PTDF/ED/PHD/OIC/848/16

Abstract

Sediment mass-balance analysis provides key constraints on stratigraphic architecture and its controls. We use the data-rich Middle Jurassic Brent Delta sediment routing system in the proto-Viking Graben, Northern North Sea, to estimate sediment budgets and mass-balance between source areas and depositional sinks. Published studies are synthesised to provide an age-constrained sequence stratigraphic framework, consisting of four previously defined genetic sequences (J22, J24, J26, J32). Genetic sequence J32 (3.9 Myr) records transverse progradation of basin-margin deltas, sourced from the Shetland Platform to the west and Norwegian Landmass to the east. Genetic sequences J24 (1.1 Myr) and J26 (0.9 Myr) record the rapid progradation and subsequent aggradation of the Brent Delta along the basin axis, sourced from the uplifted Mid-North Sea High to the south, and the western and eastern source regions. Genetic sequence J32 (2.2 Myr) records the retreat of the Brent Delta. Sediment budgets for the four genetic sequences are estimated using palaeogeographical reconstructions, isopach maps, and sedimentological analysis of core and well-log data. The estimated net-depositional sediment budget for the mapped Brent Delta system is 2.0–2.8 Mt/year. Temporal variations in net-depositional sediment budget were driven by changes in tectonic boundary conditions, such as the onset of uplift before the deposition of genetic sequence J24. Over the same time period, the Shetland Platform, Norwegian Landmass and Mid-North Sea High source regions are estimated to have supplied 2.3–5.6, 5.0–14.1, and 2.8–9.4 Mt/year of sediment, respectively, using the BQART sediment load model and independent geometrical reconstruction of eroded volumes, which are constrained by isostatic uplift estimates based on the geochemistry of syn-depositional volcanic rocks. The net-depositional sediment budget in the sink is an order-of-magnitude smaller than the total sediment budget supplied by the source regions (13.9–23 Mt/year). This discrepancy suggests that along-shore transport by wave-generated currents into

the coeval Faroe-Shetland Basin and/or down-dip transport by gravity flows into the coeval western Møre Basin played a key role in redistributing sediments away from the Brent Delta system.

KEYWORDS

Brent Delta, sediment budget, sediment mass-balance, sediment routing system, source-to-sink

1 | INTRODUCTION

Sediment routing systems dynamically link sediment source regions (e.g., erosional catchments) to depositional sinks (e.g., basin floor) via sediment transfer or dispersal conduits (e.g., rivers and slope canyons, oceanographic currents) and temporary storage zones (e.g., floodplain, coastal plain, shelf and slope; Figure 1; Allen, 2017; Sømme et al., 2009). Constraining variations in quantitative estimates of sediment influx into the system, partitioning of sediment volumes within its segments, and potential sediment export out of the primary depositional sink, can be linked to regional tectonics (e.g., orogenic uplift, fault movement), climate (e.g., water discharge, erosion rate), relative sea-level changes, autogenic behaviour (e.g., channel avulsion, delta-lobe switching), or basinal processes (e.g., waves, tides; Allen et al., 2013; Helland-Hansen et al., 2016; Hinderer, 2012; Romans et al., 2016). Furthermore, these quantitative estimates have significant economic implications, because they can provide important constraints on the volume, distribution, and quality of resource-bearing sedimentary rocks (Martinsen et al., 2010; Bhattacharya et al., 2016; Eide et al., 2017).

Sediment mass-balance analysis provides a first-order quantification of the influence of sediment supply and accommodation generation on stratigraphic architecture, and the tectonic and climatic signals with which they are associated (Paola & Martin, 2012). This approach to stratigraphic interpretation complements traditional sequence stratigraphic approaches and provide a means to critically appraise existing sequence stratigraphic frameworks (Carvajal & Steel, 2012; Gomez-Veroiza & Steel, 2017; Hampson et al., 2014). The ability to constrain sediment supply and its associated grain-size mix from the source area to the depositional sink is therefore fundamental to developing robust stratigraphic interpretations and reconstructing palaeocatchment conditions. At the basin scale, gathering data to constrain an entire ancient source-to-sink system over a range of geological timescales (>10^6 year) can be challenging, as it requires the integration of both 'source-focused' constraints on the size of the palaeocatchment, bedrock lithology, relief evolution, and palaeoclimate (Galloway et al., 2011; Lyster et al., 2020; Tinker et al., 2008) and 'sink-focused' constraints on basin architecture, tectonic subsidence, and sediment thicknesses or volumes (Grimaud

Highlights

- Sediment budgets of source areas and depositional sink are compared for well-documented Brent Delta system.
- Changes in tectonic boundary conditions controlled temporal evolution of sediment budget in depositional sink.
- Both axial and transverse drainages contributed significantly to source-area sediment budgets.
- Sediment mass supplied by source areas exceeds mass deposited in Brent Delta by an order-of-magnitude.
- Sediment dispersal from over-supplied Brent Delta is required to achieve sediment mass balance.

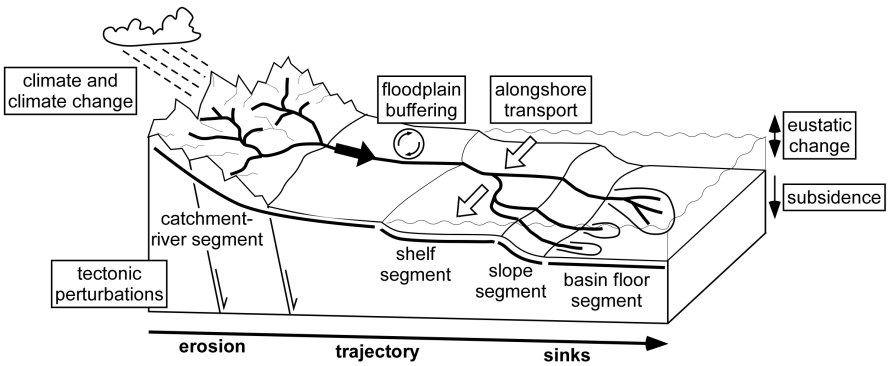

FIGURE 1 Controls and components of a typical sediment routing system, which links sediment source areas to depositional sinks (after Allen & Heller, 2011).

et al., 2018; Guillocheau et al., 2012; Hampson et al., 2014; Liu & Galloway, 1997; Lodhia et al., 2019; Walford et al., 2005) over the same time interval. Importantly, the challenges associated with incomplete preservation of ancient sediment routing systems, spatial and temporal variations in geological characteristics, sparse sampling by widely spaced well data and other dataset limitations imply that a systematic method of quantifying the probabilistic range of outcomes is needed to robustly assess uncertainties (e.g., Brewer et al., 2020; Zhang et al., 2018).

The well-studied Middle Jurassic Brent Delta sediment routing system is sufficiently data-rich to test sediment mass-balance concepts. The present-day distribution of Brent Group strata defines an important hydrocarbon province in the Northern North Sea, offshore UK and Norway, and the depositional architecture and provenance of these strata have been documented extensively (e.g., Budding & Inglin, 1981; Fjellanger et al., 1996; Gabrielsen et al., 2010; Hampson et al., 2004; Johannessen et al., 1995; Mitchener et al., 1992; Morton et al., 2004; Morton, 1992; Underhill & Partington, 1993; Ziegler, 1990). This previous work and supporting database of cores, well logs, and seismic reflection data collected over six decades of hydrocarbon exploration and production in the depositional sink provide an opportunity to test and extend the application of sediment mass-balance methods.

Although much is known about the Brent Delta sediment routing system, key allogenic controls on stratigraphic architecture (e.g., sediment supply) are still not well constrained. For example, it is unclear which of the potential provenance areas predominantly fed the Brent Delta system (Helland-Hansen et al., 1992; Husmo et al., 2002; Mitchener et al., 1992; Morton, 1992). Neither the total sediment discharge into the Brent Delta system, nor the relative contribution to the sediment budget from each source region, nor the proportion of discharged sediments preserved within the primary depositional sink are well understood. The aims of this paper are: (i) to synthesise published information on potential sediment source areas and age-constrained sequence stratigraphic framework of the sediment routing system; (ii) to estimate and compare sediment budgets for the depositional sink and potential source regions; and (iii) to assess potential drivers of temporal and spatial variations in sediment budget.

2 | GEOLOGICAL FRAMEWORK OF THE BRENT DELTA SYSTEM

2.1 | Tectono-stratigraphic context

The Viking Graben is the broadly north–south trending basin that represents the northern arm of the trilete North Sea rift system (Figure 2a,b). It is bounded to the west by the Shetland Platform, to the east by the Norwegian mainland, to the south by the Mid-North Sea High, and to the north by the Faroes-Shetland and Møre basins (Figure 2b), which form part of the present-day Atlantic Margin. The Viking Graben and surrounding Northern North Sea region is underlain by high-grade metamorphic and plutonic rocks, which were deformed by thrusts and shear zones during the Caledonian orogeny and subsequent extensional collapse of the orogenic belt (Fazlikhani et al., 2017; Gabrielsen et al., 1990; Zanella & Coward, 2003). The main structural pattern of the Northern North Sea later developed during two major lithospheric rifting episodes (Figure 2d; Barton & Wood, 1984; Duffy et al., 2015; Færseth, 1996; Phillips et al., 2019; Steel & Ryseth, 1990; Zanella & Coward, 2003): (i) Late Permian to Early Triassic rifting, which led to the development of large displacement (c. 1000 m), north–south trending faults, and (ii) Late Jurassic to Early Cretaceous rifting, which reactivated earlier north–south trending rift-related structures and generated additional northeast-southwest trending faults (Figure 2b). The timing of these rifting episodes (Figure 2d) is a matter of ongoing debate, and in particular, the Jurassic rifting may have initiated in the Middle Jurassic (latest Bajocian; Folkestad et al., 2014; Helland-Hansen et al., 1992) and continued in multiple pulses until the Volgian (earliest Cretaceous; Rattey & Hayward, 1993; Ravnås et al., 2000). Following the Triassic rifting episode, a prolonged post-rift thermal subsidence phase ensued from Late Triassic to Middle Jurassic times (Partington et al., 1993; Rattey & Hayward, 1993; Steel, 1993).

During the Middle Jurassic, uplift associated with a transient mantle plume is interpreted to have resulted in the erosion of Lower Jurassic and Triassic strata in the Mid-North Sea area, and the development of an intra-Aalenian unconformity, widely referred to as the "mid-Cimmerian Unconformity", during the early Middle Jurassic (Figure 2d; Underhill & Partington, 1994; Ziegler, 1990). Recent re-interpretation of 3D seismic reflection data suggests lava was sourced by fissure eruptions from linear vents and associated small volcanic edifices (Quirie et al., 2019). The resulting "dome" was about 700–1000 km in diameter, as inferred from the subcrop patterns of pre-Middle Jurassic strata below the "Mid-Cimmerian Unconformity", and developed near the triple junction of the trilete rift system (Figure 2b,c; Underhill & Partington, 1993). Deposition of the Brent Group coincided with this interpreted phase of thermal doming and subsequent collapse of the "dome" (Husmo et al., 2002; Underhill & Partington, 1993). Patchy, thin (typically <50 m but locally up to 200 m) Bajocian-Bathonian sandstones and mudstones are locally preserved between lavas

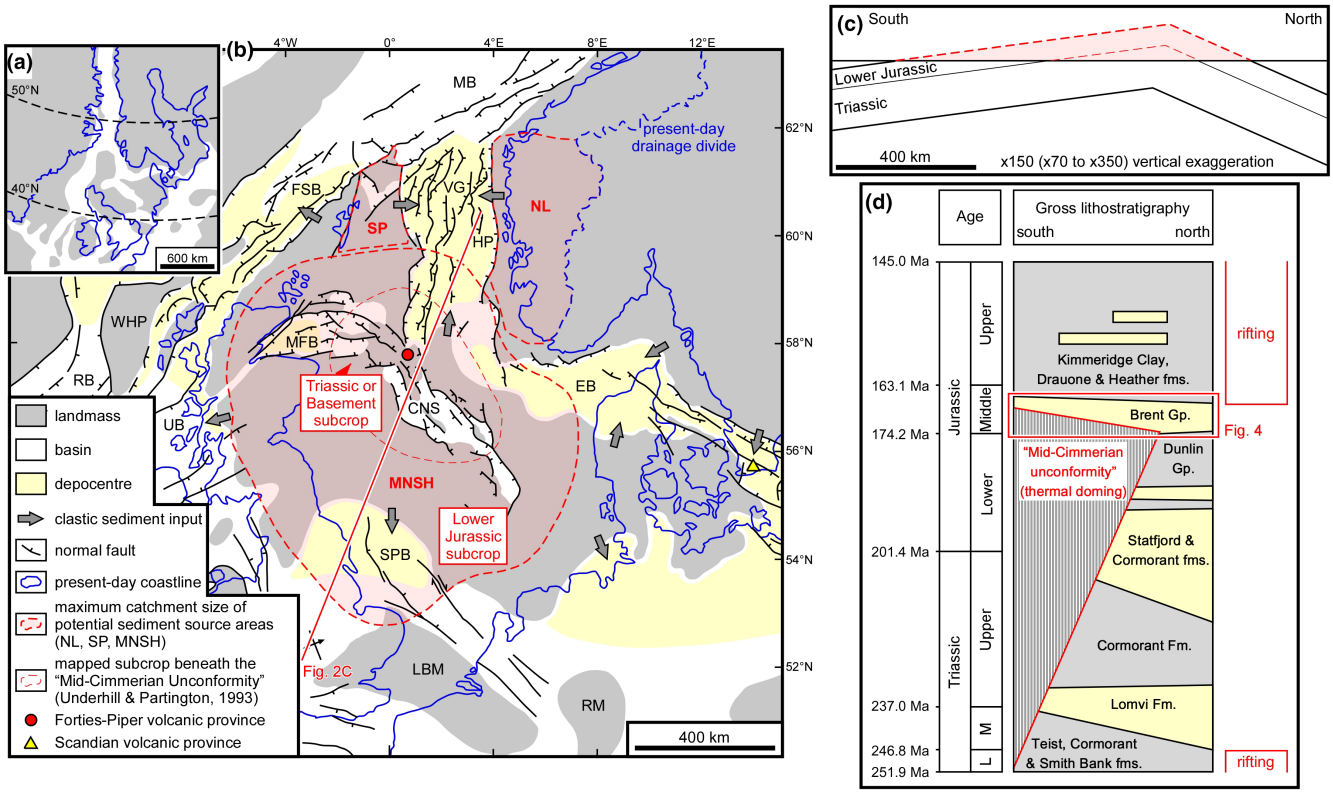

FIGURE 2 (a) Unrestored Middle Jurassic palaeogeographical reconstruction of the North Sea (Ziegler, 1990; Torsvik et al., 2002). (b) Restored Middle Jurassic palaeogeographical reconstruction of the Northern North Sea showing palaeo-landmasses and basins (Ziegler, 1990). Note the extent of the proto-Viking Graben (VG) and sediment input into the basin from the Shetland Platform (SP), Norwegian Landmass (NL), and Mid-North Sea High (MNSH). Additional tectonic elements include the Central North Sea (CNS), Egersund Basin (EB), Faroes-Shetland Basin (FSB), Horda Platform (HP), London-Brabant Massif (LBM), Moray Firth Basin (MFB), Møre Basin (MB), Rhenish Massif (RM), Rockall Basin (RB), South Permian Basin (SPB), Unst Basin (UB), West Hebrides Basin (WHP). The mapped extent of the subcrop beneath the "Mid-Cimmerian Unconformity", which formed due to initiation of the MNSH uplift (Underhill & Partington, 1993), and the Forties-Piper and Scandian volcanic provinces (Figure 7) are shown. Depocentres supplied by abundant clastic sediment occur in the Faroes-Shetland Basin (FSB), South Permian Basin (SPB), Egersund Basin (EB) and in northern Germany, in addition to the Brent Delta depocentre in the Viking Graben (VG) and Horda Platform (HP). (c) Cross-section showing a simplified geometrical restoration of eroded material over the MNSH. The eroded material approximates a cone with a height equal to the total thickness of exhumed Lower Jurassic and Triassic strata, and a cross-sectional area equal to the mapped area of the subcrop pattern (Figure 2B). (d) Simplified lithostratigraphic column for the proto-Viking Graben (Figure 2B) highlighting the main phases of structural evolution in relation to deposition of the Brent Delta sediment routing system (Figure 4; see text for details).

and volcaniclastic deposits above the "dome" (Quirie et al., 2020; Underhill & Partington, 1993).

2.2 | Source region characteristics

Three main sediment provenance regions have been interpreted for the Brent Delta sediment routing system, based on observed facies trends and thickness patterns, framework mineralogy, detrital heavy mineral (e.g., garnet) geochemistry, and isotope (e.g., strontium-neodymium) data (Hamilton et al., 1987; Hurst & Morton, 1988; Mearns, 1992; Mitchener et al., 1992; Morton, 1985, 1992; Skarpnes et al., 1980). They are the Norwegian Landmass, composed of Precambrian and Caledonian metamorphic basement, to the east; the Shetland Platform, composed of Devonian, Carboniferous and Permo-Triassic sedimentary rocks reworked from Caledonian metamorphic basement, to the west; and the Mid-North Sea High, composed of sandstone-dominated Triassic and mudstone-dominated Lower Jurassic sedimentary rocks, to the south of the Viking Graben (Figure 2b). The broad geological characteristics of these three source areas (e.g., catchment-wide bedrock lithology, size and relief) synthesised from published studies are summarised below.

The Norwegian Landmass area forms part of the Fennoscandian Shield, and is underlain mainly by Precambrian gneisses and Caledonian metamorphic and granitic rocks (Husmo et al., 2002; Morton et al., 2004; Underhill, 1998). The relief of the Norwegian Landmass

has evolved as a product of complex interactions between large-scale tectono-magmatic processes, from a Caledonian relief of up to 9 km to the present-day relief of 2 km, with significant increases and decreases linked to rift- and post-rift tectonics in the North Sea region (Gabrielsen et al., 2010; Johannessen et al., 2013; Ksienzyk et al., 2014; Smelror et al., 2007). Although the mechanisms driving post-Caledonian to Recent palaeotopographic evolution of the Fennoscandian Shield are a matter of ongoing debate (Chalmers et al., 2010; Medvedev & Hartz, 2015; Nielsen et al., 2009), there is little disagreement on the presence of kilometre-scale palaeorelief in the region during the Jurassic. Maximum relief of the Norwegian Landmass is estimated to have been 1.6 km in the Late Jurassic, during uplift of the active rift shoulder, based on application of the BQART model to Late Jurassic sediment volumes deposited offshore Norway (Sømme et al., 2013). Middle Jurassic relief is estimated to have been smaller, approximately 1 km, based on interpretation of reflection seismic, potential field and apatite fission track (AFT) data (Gabrielsen et al., 2010; Medvedev & Hartz, 2015).

The pre-Mesozoic bedrock of the Scottish Mainland, Shetland Isles and Shetland Platform is composed mainly of Precambrian metasediments, Caledonian metamorphic and granitic rocks, and Upper Palaeozoic clastic and volcanic rocks (Morton et al., 2004; Underhill, 1998; Zanella & Coward, 2003). The Shetland Platform underwent a similar evolution to the Norwegian Landmass during the Jurassic, but its palaeotopographic relief is poorly constrained.

Subcrop patterns below the "Mid-Cimmerian Unconformity" indicate that mudstone-dominated Lower Jurassic and sandstone-dominated Triassic strata were eroded from the Mid-North Sea High source region (Figure 2b,c; Underhill & Partington, 1993, 1994). The "Mid-Cimmerian Unconformity" is patchily overlain by Middle Jurassic coastal plain, shallow-marine and extrusive volcanic rocks (Husmo et al., 2002; Quirie et al., 2019, 2020). The thickness of Lower Jurassic and Triassic sedimentary rocks exhumed due to the "Mid-Cimmerian Unconformity" is estimated to be 0.7–1.3 km, based on the integrated analysis of sonic velocity, vitrinite reflectance and AFT data (Japsen et al., 2007), which is broadly consistent with stratigraphic thickness constraints from wells that suggest a missing section of 0.3 km (conservative depositional thickness of Lower Jurassic strata) to >1 km (Husmo et al., 2002). Regional uplift and palaeorelief of the Mid-North Sea High is poorly constrained in published literature, with a maximum relief of 0.4–0.5 km suggested by Underhill and Partington (1993) based on the estimated thickness of strata eroded at the "Mid-Cimmerian Unconformity". Stratal onlap patterns above the unconformity indicate that regional uplift reached its maximum lateral extent during the Aalenian (Figure 2d), and peak uplift is interpreted to have occurred in the Late Aalenian (Quirie et al., 2020) or Bathonian (Underhill & Partington, 1993). Regional palaeogeographical reconstructions suggest that sediments from the Mid-North Sea High source region were supplied radially to five major sediment routing systems in neighbouring basins, including the Moray Firth Basin to the west, Viking Graben to the north, and the South Permian Basin to the south (Figure 2b; Underhill & Partington, 1993; Ziegler, 1990). Thus, only part of the eroded sediments was supplied to the Brent Delta sediment routing system.

2.3 | Middle Jurassic palaeoclimate of the Northern North Sea

The Middle Jurassic palaeoclimate of the Northern North Sea region is interpreted to have been sub-tropical and humid, based on the study of coals, palynological data, palaeolatitude reconstruction, strontium isotope data, oxygen isotope data, and numerical simulations of ocean–atmosphere interactions (Abbink et al., 2001; Prokoph et al., 2008; Sellwood & Valdes, 2006). The mean annual temperature is estimated to have been 20°C, based on the ocean–atmosphere general circulation models of Sellwood and Valdes (2006, 2008). While some studies of floral assemblages suggest there was a warmer, semi-arid to arid climate in the Late Jurassic (Middle Oxfordian to earliest Ryazanian), due to rifting and volcanism that resulted in changes in the concentration of greenhouse gases (Abbink et al., 2001; Dera et al., 2011), other studies use marine ammonite and ostracod assemblages and oxygen isotopes to argue that the Late Jurassic was cooler over much of northwest Europe, due to a drawdown in atmospheric CO_2 by enhanced organic carbon burial (Dromart et al., 2003; Schudack, 1999). Significant change in climate did not occur throughout the Middle Jurassic, but is interpreted to have occurred at the Late Jurassic to Cretaceous transition, towards a humid, tropical climate (Ford & Golonka, 2003).

3 | DATA AND METHODS

3.1 | Dataset

Eighty four representative exploration wells which contain published interpreted sequence stratigraphic surfaces, 53 wells from offshore UK and 31 from offshore Norway, form the framework for this study (Figure 3). A total thickness of 1500 m of core was logged from eight wells to carry out sedimentological facies analysis (see

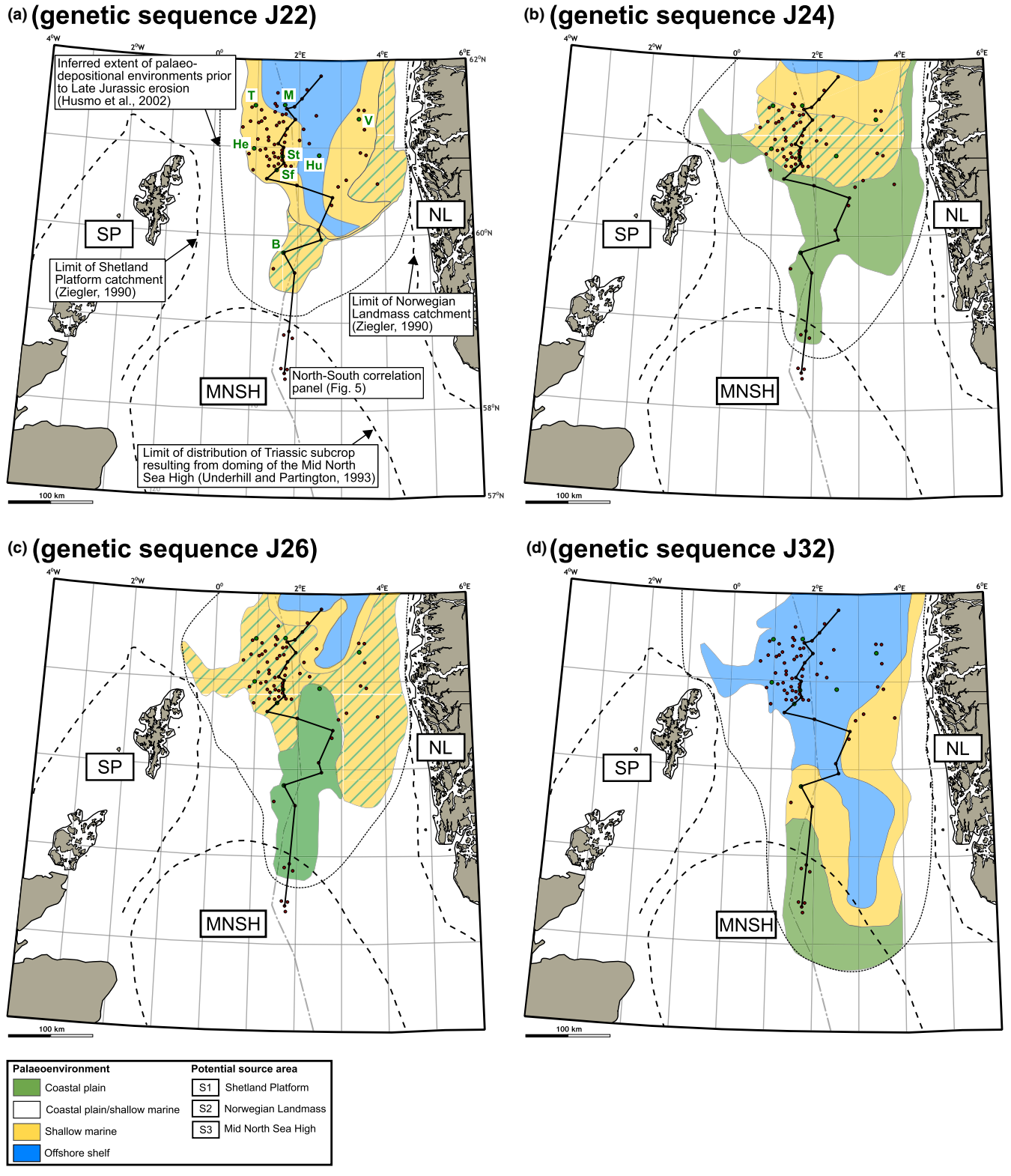

Supplementary Material for detail). The wells were selected based on their geographical spread, the thickness of the cored interval, and the variability in wireline log response, in order to capture facies associations representative of the Brent Delta sediment routing system and calibrate the lithological composition of facies associations in uncored wells.

3.2 | Method for estimating depositional-sink sediment budget

The sediment mass-balance methods applied in this study adapt established workflows proposed for assembling a sediment budget for ancient sediment routing systems (Carvajal & Steel, 2012; Hampson et al., 2014; Michael

FIGURE 3 Palaeogeographical reconstructions of the Brent Delta sediment routing system showing representative well database (red and green circles for uncored and cored wells, respectively) used for this study (modified after Mitchener et al., 1992; Fjellanger et al., 1996; Husmo et al., 2002). (a) Maximum progradation of the eastward prograding Broom Delta and westward prograding Oseberg Delta (genetic sequence J22); (b) maximum progradation of the main Brent Delta (genetic sequence J24); (c) aggradation of the main Brent Delta (genetic sequence J26); and (d) transgression and southward retreat of the main Brent Delta (genetic sequence J32). The extent of palaeo-depositional environments prior to Late Jurassic erosion is shown as dotted lines (Husmo et al., 2002). Potential sediment source areas to the west, east and south of the basin are labelled SP (Shetland Platform), NL (Norwegian Landmass) and MNSH (Mid-North Sea High), respectively, and the extent of the source areas are constrained by published literature (Ziegler, 1990; Underhill & Partington, 1993). The locations of eight cored wells used for facies characterisation (see Supplementary Material for details) are shown: B – 9/9b-3 (Bruce Field), He – 2/5–3 (Heather Field), Hu – 30/2–2 (Huldra Field), M – 211/19–6 (Murchison Field), Sf – 3/8b-10 (Staffa Field), St – 3/4a-12 (Strathspey Field), T – 210/20–2 (Tern Field), V – 35/8–1 (Vega Field). A regional stratigraphic correlation line (Figure 5) is also located.

et al., 2014; Rohais & Rouby, 2020). The six steps involved in compiling the net-depositional sediment budget in the sink(s) are as follows:

(i) A regionally consistent, age-constrained stratigraphic framework for the depositional sink was synthesised from published studies, to subdivide the Brent Delta system into four age-constrained genetic sequences (sensu Galloway, 1989) of different durations (Figures 4 and 5).
(ii) Sedimentary facies analysis was carried out to calibrate wireline-log signatures to sediment grain-size characteristics and facies proportions (see Supplementary Material for details), and to constrain the distribution of coastal plain, marginal marine, and shallow-marine to shelf segments of the sediment routing system (Figure 5).
(iii) Isopach maps were generated for each time interval by interpolating thickness contours between studied well data points (Figure 6). Biogenic rocks (e.g., coals) were discounted in thickness estimation. The boundaries of the sediment routing system, maximum sediment thicknesses and proportion of subsequently eroded volumes are constrained by published seismically derived isopach maps for the Middle Jurassic unit (Husmo et al., 2002; Mitchener et al., 1992).
(iv) For each stratigraphic interval, net-depositional sediment volumes are calculated using the isopach maps. Sediment volumes are converted to masses by using a range of lithology-specific bulk-density values obtained from geophysical density logs, which accounts for both porosity loss due to compaction and any internally derived cement in the rock, generated by alteration of framework grains and local diffusion of carbonate during burial (cf. Carvajal & Steel, 2012; Hampson et al., 2014).
(v) The sink-derived net-depositional sediment budget, presented in mass per unit time, was estimated by dividing the calculated sediment mass with the duration for each unit as defined by the stratigraphic framework (Figure 4). The boundaries of each stratigraphic unit have been assigned absolute ages using the current Geologic Time Scale (Gradstein et al., 2012; Ogg et al., 2016).
(vi) The relative contribution of the three sediment source regions (Section 2.2) to net-depositional sediment volumes was estimated using garnet compositional data that distinguish a characteristic sandstone provenance for each sediment source region (Morton, 1992).

3.3 | Methods for estimating source-area sediment budget

The long-term averaged budget of sediment supplied by the erosional source-area(s) was quantified using two independent methods, where sufficient data are available.

In the first method, we applied the BQART model of Syvitski and Milliman (2007) to the three distinct source areas. The BQART model describes an empirical relationship between measured suspended sediment loads in 488 modern catchments and their source-area characteristics, such as climate, bedrock lithology, palaeocatchment area and relief (Milliman & Farnsworth, 2011; Milliman & Meade, 1983; Milliman & Syvitski, 1992; Syvitski & Milliman, 2007; Syvitski et al., 2003). The BQART model (Syvitski & Milliman, 2007) is expressed as:

$$Q_s = 0.0006 B Q_w^{0.31} A^{0.5} R T \quad (\text{for } T \geq 2°\text{C}), \tag{1}$$

where Q_s is sediment load (Mt/year; 1 Mt = 10^9 kg), Q_w is water discharge (km^3/year), A is catchment area (km^2), R is maximum catchment relief (km), and T is catchment-averaged temperature (°C).

Q_w is estimated as the product of catchment area and runoff, and is given as (Milliman & Farnsworth, 2011):

$$Q_w = A\, r, \tag{2}$$

where r is runoff (km/yr).

Milliman and Farnsworth (2011) proposed four climate zones characterised by different runoff values, based on modern systems. For a humid climate zone, r is 250–750 mm/year. The calculated range of values for water discharge using this relationship is consistent with values calculated using the empirical equations of both Syvitski and Milliman (2007) and Eide et al. (2018) for a humid climate zone. Input values for other parameters (A, R, and T) are constrained by previously published palaeogeographical reconstructions, structural restorations, thermochronological and palaeoclimate modelling studies, as summarised previously (Section 2.2).

The dimensionless B term broadly encompasses bedrock erodibility, for which Syvitski and Milliman (2007) consider that the catchment-averaged lithology factor, L, is a key variable, alongside any glacial cover in the source areas, anthropogenic influence and in-catchment sediment storage. For the assessment of the Middle Jurassic Brent Delta system, there was no glacial cover in the source areas, and anthropogenic influence was non-existent. No studies suggest that significant sediment volumes were trapped in hinterland catchments. Consequently, we make the following assumption:

$$B \sim L \tag{3}$$

where L is taken from the values presented for different rock-type classes in Syvitski and Milliman (2007). For our study, dominant catchment lithologies are determined from previous palaeogeographical reconstructions and provenance studies (Section 2.2). Assigning different values of L to catchments that have markedly distinct dominant lithologies is a reasonable assumption within a BQART framework, because different bedrock lithologies can influence erodibility and, therefore, the suspended sediment budget (Carroll et al., 2006; Zondervan et al., 2020). Accordingly, L is varied between 0.5 for crystalline basement to 2.0 for clastic sediments, consistent with the methodology of Syvitski and Milliman (2007), but we acknowledge that choosing single values for lithology factors is challenging (e.g., Wapenhans et al., 2021).

The second method involved a simple geometrical reconstruction of the eroded section of the Mid-North Sea High, above the mapped subcrop patterns of Lower Jurassic and Triassic units below the "Mid-Cimmerian Unconformity" (Figure 2b; Underhill & Partington, 1993). The reconstructed volume of eroded material approximates the shape of a spherical dome (Figure 2c), with the area of the base of the dome approximately equal to the mapped area of Lower Jurassic and Triassic subcrop (Underhill & Partington, 1993), and the height of the dome equal to the total thickness of exhumed Lower Jurassic and Triassic units estimated from published studies (Figure 2c; Husmo et al., 2002; Japsen et al., 2007). Eroded sediment volume is converted to sediment mass, using a bulk-density of 2.0–2.4 g/cm^3, to account for compaction of sediments buried to 0.3–1.3 km depth prior to exhumation (Section 2.2; e.g., Sclater & Christie, 1980). The sediment budget is estimated by dividing the sediment mass with the total duration of exhumation of the Mid-North Sea High from Aalenian – Early or Late Callovian (8–10 Myr duration; Underhill & Partington, 1993, 1994). Sediment eroded from the Mid-North Sea High was supplied to five depocentres that are arranged radially around the perimeter of the high, in the Faroes-Shetland Basin, South Permian Basin, Egersund Basin, Viking Graben and Horda Platform, and in northern Germany (Figure 2b). We therefore estimate that approximately one-fifth (10%–30%) of the sediment eroded from the Mid-North Sea High was supplied northwards to the Brent Delta sediment routing system in the Viking Graben and Horda Platform, and the rest was routed into the other four depocentres.

3.4 | Method for constraining uplift of the Mid-North Sea high

We exploit the geochemical compositions of previously published basaltic samples from across the Mid-North Sea High (MNSH) volcanic region to constrain the thermal structure of the uppermost mantle at the time of rifting, and calculate isostatic support in two locations (Figure 2b): (i) the centre of the MNSH (Forties-Piper province, UK) that directly feeds into the Brent Delta system, with an estimated $^{40}Ar/^{39}Ar$ age of 155 ± 5 Ma (Latin, 1990; Latin & Waters, 1992), and, for comparison, (ii) the margin of the MNSH, about 700 km southeast of the Forties-Piper province (Scanian province, southern Sweden), with an estimated $^{40}Ar/^{39}Ar$ age of 176.7 ± 0.5 Ma (Tappe et al., 2016).

We estimate mantle potential temperature (T_p) and lithospheric thickness (L_t) at the time of volcanic activity in the Forties and Scanian provinces using two independent methods that exploit the geochemical compositions of basaltic rocks: a rare-earth element melting model (INVMEL; McKenzie & O'Nions, 1991), and a whole-rock thermobarometer (PF2016; Plank & Forsyth, 2016). INVMEL estimates T_p and L_t by reducing misfit between observed rare-earth element concentrations and those calculated using a peridotitic adiabatic melting model. PF2016 are empirical equations that estimate the pressure and temperature of final mantle-melt equilibration. These equilibration results can be fit using adiabatic melting models to estimate T_p, and the shallowest equilibration results are assumed to represent the base of the lithosphere. Detailed set up for the INVMEL and PF2016 methods are

described in Ball et al. (2021) and McNab et al. (2018), respectively.

Following Ball et al. (2021), if we assume that the effect of density on pressure is negligible and that equilibrated lithospheric thickness (a_o) is 120–150 km, at sea-level, uplift, U, for the central and marginal locations in the MNSH region is calculated such that

$$U = \frac{\alpha T_1}{1-\alpha T_1}\left(\frac{a_1^2}{2a_\circ} + \frac{a_\circ}{2} - a_1 + \frac{\Delta T}{T_1}h\right), \quad (4)$$

where thermal expansivity, α, is $3\times10^{-5}°C^{-1}$, background asthenospheric temperature, T_1, is 1390°C, ΔT is excess asthenospheric temperature of thickness h. a_1 is thickness of lithosphere beneath the MNSH provinces when it was being uplifted. Uplift occurs where the lithosphere is thinned or the asthenosphere is heated.

3.5 | Error and uncertainty

The methods outlined above to estimate sediment budgets derived from the depositional sink(s) and erosional source area(s) have multiple sources of error, arising from measurement accuracy, and uncertainty, arising from the use of sparse data distributions. Uncertainties of predicted sediment budgets have been estimated by propagating observational errors using a Monte Carlo approach. Following Zhang et al. (2018) and Brewer et al. (2020), random parameter values were extracted from defined distributions and inserted into the model. For each input parameter, the range of values and their assumed probability distributions are constrained by their geological characteristics synthesised from previous studies or from data used in this study (Tables 1 and 2). Three types of probability distributions are assigned to the input parameters depending on the quality and quantity of available data. Where both maximum and minimum values for the range of input parameters are equally probable (e.g., runoff, r), a uniform distribution was chosen; where only the most probable (mean) constraint is available or calculated (e.g., catchment area, A; catchment-averaged temperature, T; mapped area of depositional sink), a normal distribution and standard deviation from the mean was assumed. Where the most probable (mean or mode) constraint is available together with additional constraints on maximum and minimum values for the range of input parameters (e.g., relief, R; catchment-averaged lithologic factor, L), a triangular distribution was chosen (cf. Brewer et al., 2020; Nyberg et al., 2021; Zhang et al., 2018). A large number of simulated realisations was generated (10,000 trials in this study) to robustly assess associated uncertainties. In this study, the quoted range of estimates represents the 10th percentile (P10) and 90th percentile (P90) probability values, while the base estimate for comparison is the median (P50) value.

4 | CONSTRUCTION OF STRATIGRAPHIC FRAMEWORK

Regional, basin-scale studies of the Middle Jurassic (Aalenian – Bathonian) succession (Bullimore & Helland-Hansen, 2009; Fält et al., 1989; Fjellanger et al., 1996; Graue et al., 1987; Hampson et al., 2004; Helland-Hansen et al., 1992; Johannessen et al., 1995; Mitchener et al., 1992; Sneider et al., 1995) present sequence stratigraphic frameworks calibrated to biostratigraphic schemes that tie marginal-marine palynostratigraphic to marine ammonite zones (Partington et al., 1993; Simon Petroleum Technology Ltd, 1994; Whitaker et al., 1992). The absolute ages of the ammonite zones are constrained by radiometric age data published in recent geological time scales (Gradstein et al., 2012; Ogg et al., 2016). It is worth noting that the total duration of the Middle Jurassic (Aalenian – Bathonian) has decreased from 22 Myr in the original publication of Mitchener et al. (1992) to 8 Myr using the revised geological time scale of Ogg et al. (2016). Regional studies are complemented by high-resolution sequence stratigraphic studies of individual fields (e.g., Brown & Richards, 1989; Budding & Inglin, 1981; Flint et al., 1998; Jennette & Riley, 1996; Livera & Caline, 1990; Løseth & Ryseth, 2003; Morris et al., 2003; Reynolds, 1995).

These frameworks are broadly consistent with one another but assign varying degrees of significance to different types of interpreted key stratigraphic surfaces, such as maximum flooding surfaces, transgressive surfaces, and sequence boundaries (Figures 4 and 5). The published age-constrained frameworks were synthesised, and their interpretations are supplemented by additional sedimentological data (see Supplementary Material for details). Confidence in this synthesised sequence stratigraphic framework is provided by: (i) use of a consistent published biostratigraphic scheme; (ii) consistency of key stratigraphic surfaces interpreted in different published frameworks in reference wells, and (iii) consistency of well correlations along depositional dip and strike sections. Our stratigraphic framework for the Brent Group and time-equivalent strata contains four stratigraphic units, which correspond to the "J sequences" proposed by Mitchener et al. (1992); each "J sequence" is a genetic sequence (sensu Galloway, 1989) bounded by biostratigraphically calibrated maximum flooding surfaces of basinwide extent (Partington et al., 1993). We briefly summarise these units below.

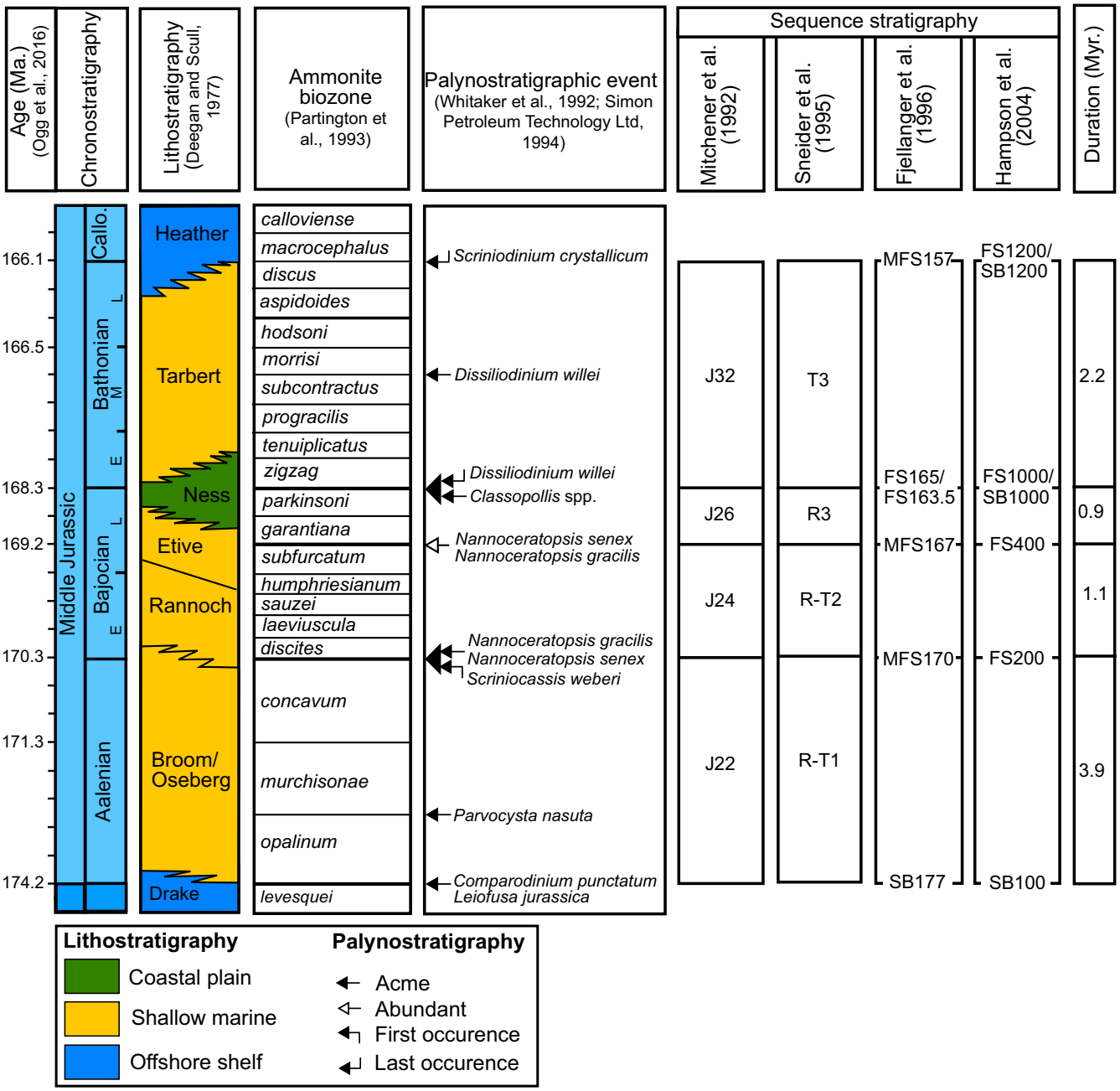

FIGURE 4 Sequence stratigraphic framework for the Brent Delta sediment routing system synthesised from various published references (Deegan & Scull, 1977; Mitchener et al., 1992; Partington et al., 1993; Sneider et al., 1995; Johannessen et al., 1995; Fjellanger et al., 1996; Hampson et al., 2004). The numbered "J sequences" of Mitchener et al. (1992) are used in this study.

4.1 | Genetic sequence J22 (Aalenian: 174.2–170.3 Ma)

The base of genetic sequence J22 is defined in much of the northern North Sea by an unconformity, which locally removed the underlying J22 maximum flooding surface, and an abrupt basinward shift of facies belts. Both of these features have been attributed to Late Toarcian uplift of the Mid-North Sea High dome, resulting in a significant fall in relative sea-level in the area around the dome (Mitchener et al., 1992; Underhill & Partington, 1993). The unit is characterised by eastward and westward regression of shallow-marine fan-delta and fluvio-estuarine deposits of the Broom and Oseberg formations, respectively, along approximately north–south-oriented palaeoshorelines (Figures 3a and 4). These characteristics are not consistent with uplift of the Mid-North Sea High dome, but instead imply renewed uplift of the inherited Triassic rift shoulders, that is the Shetland Platform and Norwegian Landmass (e.g., Helland-Hansen et al., 1992; Steel, 1993;

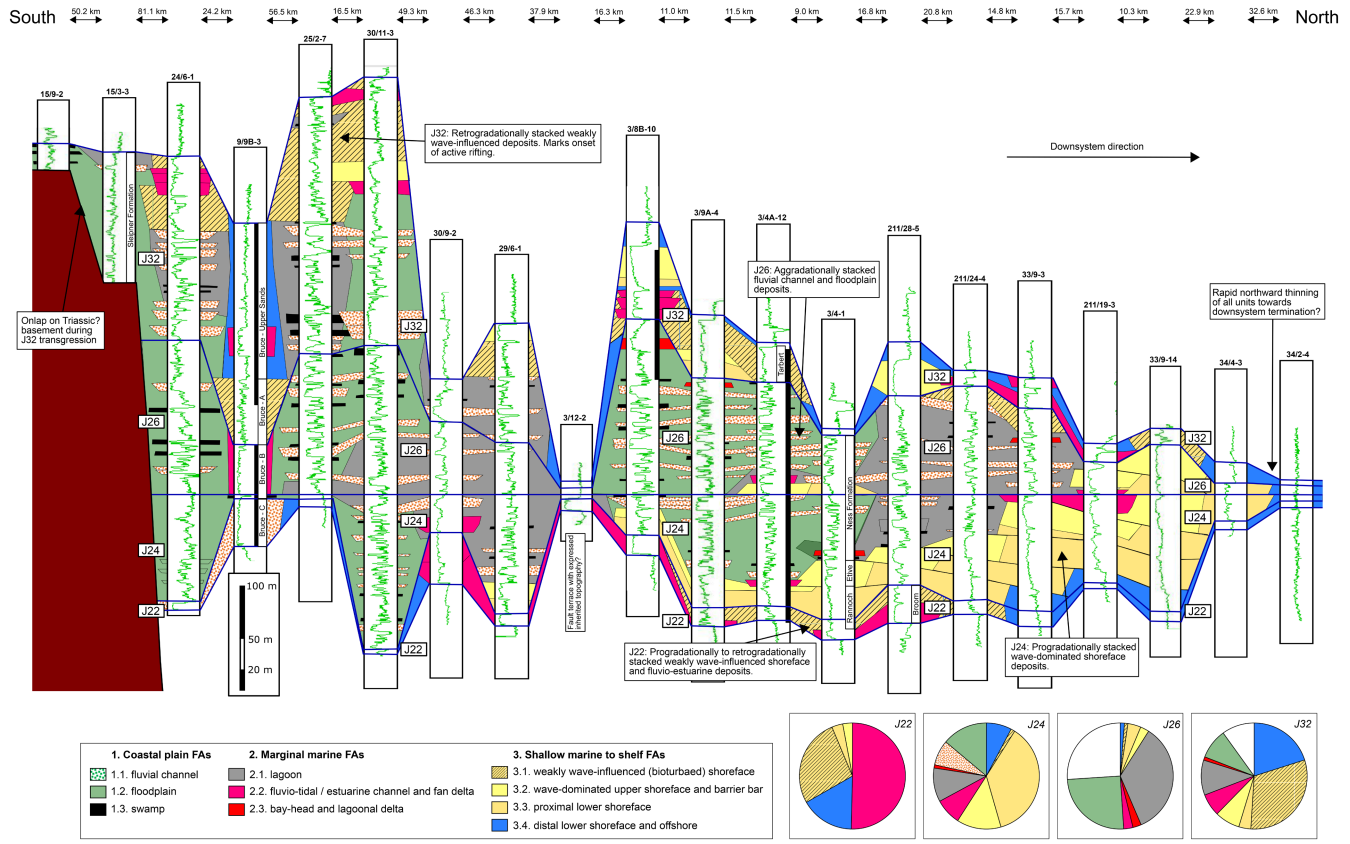

FIGURE 5 Transverse (South – North) regional sequence stratigraphic correlation along the basin (located in Figures 3 and 6), flattened on the top of the J24 unit. Given the large well spacing, only stratigraphic surfaces bounding genetic sequences J22, J24, J26 and J32 (Figure 4) are shown. Pie charts (bottom right) show the proportion of facies associations in genetic sequences J22, J24, J26 and J32, based on core and wireline-log data from 84 representative wells (see Supplementary Material for details).

Figure 3a). There is little evidence for intrabasinal fault activity during this time interval, and observed abrupt thickness changes have been attributed to passive infilling of inherited rift topography, for example across the Ninian-Hutton fault system (Hampson et al., 2004; Mitchener et al., 1992). Following regression, transgression resulted in the development of the J24 maximum flooding surface at the top of genetic sequence J22, expressed by thin marine mudstones over most of the basin, and a laterally extensive coal across the Bruce-Beryl embayment (indicated by the Bruce Field, B, in Figure 3a; Fjellanger et al., 1996; Mitchener et al., 1992). Lithostratigraphically, genetic sequence J22 broadly corresponds to the Broom Formation in the UK Brent province, the Oseberg Formation in the Norwegian sector, and the Bruce C-sand and B-C Coals in the southwestern part of the study area (Bruce-Beryl embayment). These dominantly coarse-grained deposits generally interfinger with and pass downdip into offshore shelf mudstones of the Drake Formation.

The proportions of facies associations in the well database for this genetic sequence are 0%, 50% and 50% for coastal plain, marginal marine, and shallow-marine to shelf palaeoenvironments, respectively (Figure 5). Genetic sequence J22 is relatively thin (<60 m), with a thickness of up to 80 m in major fault-bounded depocentres in the Oseberg area, around Norwegian Block 35/11 (Figure 6a).

4.2 | Genetic sequence J24 (early Bajocian: 170.3–169.2 Ma)

The base of genetic sequence J24 is defined by the J24 maximum flooding surface that caps sequence J22. A basinward shift in facies belts, and the establishment of an approximately east–west trending palaeoshoreline at the time, records the main progradation phase of the Brent Delta system (Figures 3b and 4). This basinward shift is generally interpreted to have resulted from continued uplift of the Mid-North Sea High dome and increased sediment supply from the south that outpaced the slow regional rate of relative sea-level rise, leading to rapid northward progradation (Fjellanger et al., 1996; Mitchener et al., 1992); however, local accumulation of Bajocian strata above the "dome" (Quirie et al., 2020) indicates that uplift may not have been so widespread. Genetic sequence J24 consists mainly of progradational to aggradational

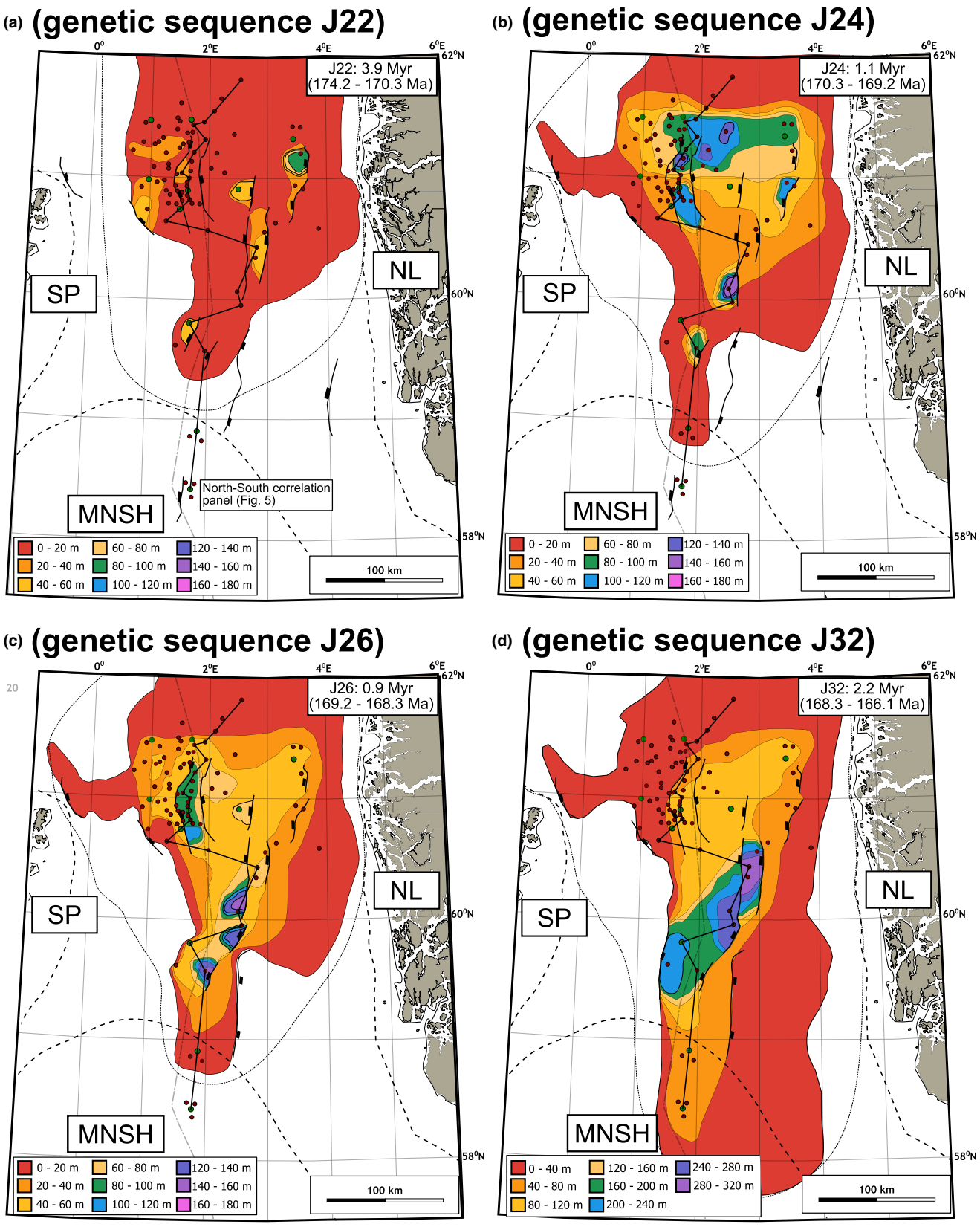

FIGURE 6 Isopach maps for four stratigraphic units, generated from the well data and constrained by published seismically derived isopach maps of Middle Jurassic strata (Mitchener et al., 1992; Husmo et al., 2002). The extent of the isopach contours, palaeo-deposition prior to Late Jurassic erosion (dotted lines), and source areas SP (Shetland Platform), NL (Norwegian Landmass) and MNSH (Mid-North Sea High) (dashed lines) are constrained by published palaeogeographical reconstructions in Figure 3: (a) genetic sequence J22; (b) genetic sequence J24; (c) genetic sequence J26; and (d) genetic sequence J32.

TABLE 1 Summary of input data, sources, and range of uncertainties for estimating depositional sink sediment budget in this study.

Input parameter	Data	Source(s) of uncertainty	Parameter value		Probability distribution
			Base value	Range	
Mapped area (km^2)	Palaeogeographical maps	Distribution, type and quality of data used in reconstructing palaeogeographical maps and sediment routing system fairway	Measured from palaeogeographical maps of the depositional sink	±20% standard deviation	Normal
Thickness (m)	Isopach maps	Distribution and representativeness of preserved interval thickness; thickness of eroded sediments	Mid-point of isopach-contour interval	Boundaries of isopach-contour interval	Triangular
Bulk density (g/cm^3)	Geophysical bulk-density log	Representativeness and quality of bulk-density log data; variations in lithology, compaction and porosity	Conglomerates and sandstones: $2.4\,g/cm^3$ Mudstones: $2.5\,g/cm^3$	$2.2–2.6\,g/cm^3$ $2.5–2.7\,g/cm^3$	Triangular
Age duration (Myr)	Biostratigraphic, radiometric and isotope data	Distribution and quality of biostratigraphic data used in defining stratigraphic boundaries; method of assigning absolute ages on the geological timescale	Absolute age assigned for boundaries of stratigraphic units	±0.5–0.7 Myr standard deviation, depending on stratigraphic boundary	Normal

shallow-marine deposits, with extensive marginal marine and coastal plain deposits that accumulated behind the shoreline (Mitchener et al., 1992; Figures 3b and 4). The top of genetic sequence J24 is marked by a sub-regional, marginal-marine mudstone ("Mid Ness Shale") that corresponds to the J26 maximum flooding surface, possibly reflecting that the rate of relative sea-level rise outpaced the rate of sediment supply (Mitchener et al., 1992). Again, there is evidence of only localised intrabasinal fault movement during the deposition of genetic sequence J24 (e.g., Folkestad et al., 2014). Lithostratigraphically, genetic sequence J24 broadly corresponds to the Rannoch and Etive formations, which comprise wave-dominated shoreface and barrier deposits, and, in most parts of the basin, the lower part of the Ness Formation, which comprises coastal plain and marginal marine deposits.

The proportions of facies associations in the well database for this genetic sequence are 22%, 19% and 59% for coastal plain, marginal marine, and shallow-marine to shelf palaeoenvironments, respectively (Figure 5). Genetic sequence J24 has a maximum thickness of 180 m, rapidly thinning beyond the northern limit of the Brent Delta shoreline at its maximum regression (Figures 3b and 6b).

4.3 | Genetic sequence J26 (late Bajocian: 169.2–168.3 Ma)

Genetic sequence J26 comprises an aggradational to slightly retrogradational succession, above the J26 maximum flooding surface. A rapid northward progradation and basinward shift in facies belts re-established a wave-dominated shoreline just south of the previous J24 maximum regressive palaeoshoreline, which later retreated and was finally drowned by marine flooding and development of the J32 maximum flooding surface in the latest Bajocian (Fjellanger et al., 1996; Mitchener et al., 1992; Figures 3c and 4). There is evidence for only localised active extensional syn-depositional faulting (e.g., Folkestad et al., 2014), and differential subsidence across remnant Triassic faults does not appear to have influenced the gross palaeogeography (Mitchener et al., 1992). Genetic sequence J26 comprises mainly coastal plain deposits in its lower part, with marginal marine deposits dominating its upper part (Hampson et al., 2004). Lithostratigraphically, genetic sequence J26 broadly corresponds to the upper part of the Ness Formation over most of the proto-Viking Graben, and the Bruce B sands and Coaly Facies in the Bruce-Beryl embayment area.

The proportions of facies associations in the well database for this sequence are 51%, 40% and 9% for coastal plain, marginal marine, and shallow-marine to shelf palaeoenvironments, respectively (Figure 5). Genetic

TABLE 2 Summary of input parameter values and associated probability distribution for estimating source-area sediment budget, using the BQART and geometrical reconstruction models (see details in sections 3.3 and 3.4). σ–standard deviation.

Source-area	Input parameter	Parameter value		Probability distribution
		Base value (mean or mode)	Range	
	BQART model			
Norwegian Landmass	Catchment lithology factor	0.5	0.25–0.75	Triangular
	Runoff (mm/year)	—	250–750	Uniform
	Catchment area (km^2)	8.1×10^4	±20% σ	Normal
	Maximum catchment relief (km)	1.2	1–3	Triangular
	Catchment-averaged temperature (°C)	20	±2 σ	Normal
Shetland Platform	Catchment lithology factor	1	0.75–1.5	Triangular
	Runoff (mm/year)	—	250–750	Uniform
	Catchment area (km^2)	2.1×10^4	±20% σ	Normal
	Maximum catchment relief (km)	1.0	0.5–1.5	Triangular
	Catchment-averaged temperature (°C)	20	±2 σ	Normal
Mid-North Sea High	Catchment lithology factor	2	1.5–2.5	Triangular
	Runoff (mm/year)	—	250–750	Uniform
	Catchment area (km^2)	4.6×10^5	±20% σ	Normal
	Maximum catchment relief (km)	0.3	0.1–0.6	Triangular
	Catchment-averaged temperature (°C)	20	±2 σ	Normal
	% delivered to Brent Delta system	20%	10%–30%	Triangular
	Geometrical reconstruction model			
Mid-North Sea High	Catchment area (km^2)	4.6×10^5	±20% σ	Normal
	Exhumed Lower Jurassic thickness (km)	0.4	0.3–0.5	Triangular
	Exhumed Triassic thickness (km)	0.3	0–1.0	Triangular
	Total exhumed unit (km)	0.7	0.3–1.5	Triangular
	Bulk-density (g/cm^3)	2.2	2–.4	Triangular
	Uplift duration (Myr)	—	8–10	Uniform
	% delivered to Brent Delta system	20%	10%–30%	Triangular

sequence J26 exhibits a similar thickness pattern to the underlying genetic sequence J24, and rapidly thins beyond the northern limit of the Brent Delta shoreline at its maximum regression (Figures 3c and 6c).

4.4 | Genetic sequence J32 (Bathonian: 168.3–166.1 Ma)

Genetic sequence J32 records the retrogradation and drowning of the Brent Delta, is bounded by the J32 and J34 maximum flooding surfaces, and is widely interpreted as a response to the onset of active rifting in the basin (Hampson et al., 2004; Mitchener et al., 1992). Palaeoshorelines evolved from an east–west to a north–south orientation, parallel to major fault trends in the basin (Figures 3d and 4). Evidence to suggest that the J32 unit records the initial phase of active extensional faulting in the basin is present in the form of pronounced sediment thickening into the hanging-walls of major faults, significant time gaps across unconformities confined to footwall crests and rift shoulders, onlap on to rift-generated topography, and the extrusion of volcanic rocks on the Mid-North Sea High (Mitchener et al., 1992; Quirie et al., 2019, 2020). Genetic sequence J32 generally consists of net-transgressive coastal plain, marginal marine, and shallow-marine to shelf deposits, including fan-delta deposits locally, that pass upwards into offshore shelf mudstones (Mitchener et al., 1992; Hampson et al., 2004). Genetic sequence J32 broadly corresponds to the Tarbert and lower Heather formations over most of the North Viking Graben, to the Bruce A and Upper Sands in the Bruce-Beryl embayment, and to the Sleipner Formation in the South Viking Graben (Husmo et al., 2002).

The proportions of facies associations in the well database for this genetic sequence are 19%, 19% and 62% for coastal plain, marginal marine, and shallow-marine to shelf palaeoenvironments, respectively (Figure 5). Genetic sequence J32 is relatively thick, reaching thicknesses of up to 320 m in the hanging-wall depocentres of major faults (Figure 6d).

5 | APPLICATION OF SEDIMENT BUDGET ESTIMATION METHODS

5.1 | Estimation of depositional-sink sediment budget

We apply the six-step method outlined above (Section 3.2) to estimate the net-depositional sediment budget of the Brent Delta sediment routing system. The construction of a regionally consistent, age-constrained stratigraphic framework from source to sink (step i; Figures 4 and 5) is described above, and the lithological characteristics and proportions of facies associations were analysed in the dataset of 84 representative wells for each of the four genetic sequences (step ii; Supplementary Material). Isopach maps illustrate the main depocentres and areal extent of each genetic sequence (step iii; Figure 6). These isopach maps and the lithological composition of each genetic sequence are used as input data to calculate sediment volumes, which are then converted to sediment masses using lithology-dependent bulk-density values (step iv; Table 1). Sediment mass values are divided by genetic sequence duration to calculate the net-depositional sediment budget in mass per unit time (step v; Table 1).

Errors and uncertainties in the estimated net-depositional sediment budgets principally derive from input parameters in the: (i) net-depositional sediment volume, which integrates the mapped area of the depositional sink and thickness from isopach maps; and (ii) absolute ages at the boundaries of the four genetic sequences. The range of input parameter values and their assigned probability distributions are summarised in Table 1. The mapped area is assigned a normal distribution with a mean value obtained from mapped area of the depositional sink and a standard deviation of ±20% of the mapped area, in order to account for inherent uncertainties in well data coverage and published maps used for reconstructing palaeogeographical extent. Grid thickness in the isopach map is assigned a triangular distribution with a range equal to the lower and upper boundary of the contour interval and a mode equal to the mid-point of the contour interval (e.g., for a 20–40 m isopach-contour interval, the minimum and maximum values are 20 and 40 m, respectively, with a mode of 30 m). Bulk-density is also assigned a triangular distribution with lithology-specific mode and range of values obtained from the geophysical bulk-density logs. The absolute ages of the boundaries of each genetic sequence are assigned a normal distribution with a mean and standard deviation obtained from published geological timescales tied to the biostratigraphic ages that constrain the genetic sequence boundaries (Gradstein et al., 2012; Ogg et al., 2016).

5.2 | Estimation of source-area sediment budget

The value ranges and distributions of five input parameters (B, Q_w, A, R, and T) are estimated in applying the BQART model to assess the budget of sediment supplied by the erosional source-areas in the Norwegian Landmass, Shetland Platform, and Mid-North Sea High (Equations 1–3; Table 2, based on published constraints outlined in Section 2.2 and summarised below). The catchment lithology factor, represented as $B = L$, is assigned a triangular distribution with a range and mode consistent with the dominant catchment-averaged lithology (Table 2). Using the compilation of Syvitski and Milliman (2007), modal values assigned to L are 0.5 for dominant high-grade metamorphic and granitic bedrock (Norwegian Landmass; Husmo et al., 2002; Morton et al., 2004; Underhill, 1998), 1.0 for a mixture of metamorphic and sedimentary bedrock lithologies (Shetland Platform; Husmo et al., 2002; Morton et al., 2004), and 2.0 for dominant sedimentary bedrock (Mid-North Sea High; Underhill & Partington, 1993, 1994). Water discharge, Q_w, represented as runoff, r, is assigned a uniform distribution with a range of 250–750 mm/year for a humid climate, for all three source areas. Catchment area, A, is assigned a normal distribution with a mean value obtained from compiled palaeogeographical maps and a standard deviation of ±20% that represents uncertainties in palaeogeographies which are difficult to quantify formally (Figure 2b; Underhill & Partington, 1993, 1994; Ziegler, 1990). Mean values of A for the Norwegian Landmass, Shetland Platform and Mid-North Sea High are 81,000, 21,000 and 460,000 km^2, respectively. For all three source areas, the catchment-averaged temperature, T, is assigned a normal distribution with a mean value of 20°C for a humid, subtropical Middle Jurassic climate (Sellwood & Valdes, 2006, 2008). We assume a standard deviation of ±2°C for this temperature distribution, to account for local climatic variations and modelling uncertainties (Table 2), consistent with palaeoclimate models (Sellwood & Valdes, 2006, 2008).

Uplift and relief of the Mid-North Sea High (MNSH) region is constrained by results of our INVMEL and

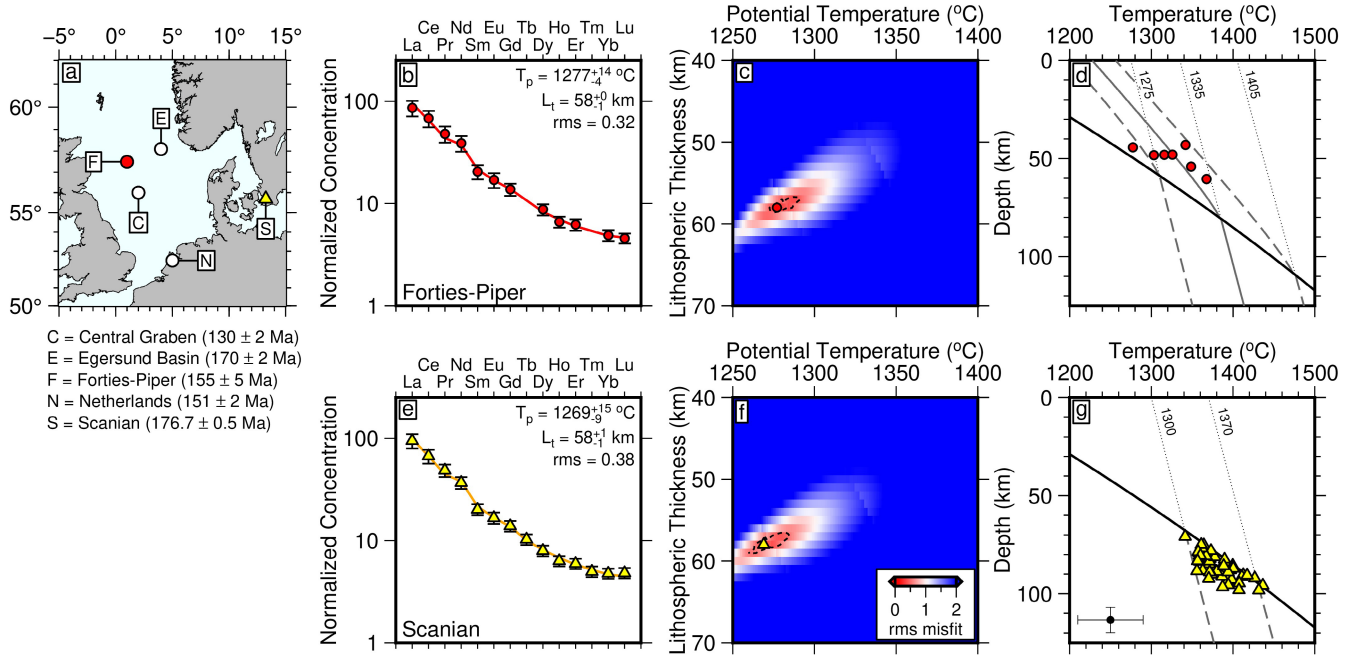

FIGURE 7 Mesozoic North Sea magmatism. (a) Map of North Sea region; coloured symbols = loci of igneous provinces with lettered boxes corresponding to names and ages of provinces listed below. (b–g) Compositional data and estimates of potential temperature, lithospheric thickness, and temperature and depth of equilibration for (b–d) the Forties-Piper volcanic province and (e–g) the Scandian volcanic province. (b, e) Circles with vertical bars = average element concentrations (ppm) ± 1 sigma for samples with >8.5 wt% MgO. Coloured line = element concentrations for INVMEL model that best fits the data using methodology as described in Ball et al. (2021). Optimal values of potential temperature (T_p) and lithospheric thickness (L_t) for models that are within ±1.5 times minimum model misfit and minimum rms misfit are shown top right. (c, f) Root mean square (rms) misfit between observed and INVMEL-calculated element concentrations as function of T_p and L_t. Coloured symbol = loci of optimal model; dashed line = limit of all models with rms values ±1.5 times minimum rms misfit. (d, g) Coloured symbols = temperature and depth of equilibration for each sample with >8.5 wt% MgO using Plank and Forsyth (2016) thermobarometer. Equilibration results calculated using samples back-calculated to Mg = 90 and using Fe(3+) Sigma Fe = 0.15 and H_2O = 200 times Ce concentration of sample. Black line = anhydrous solidus; solid grey line = best-fitting melt pathway to equilibration data; dashed grey lines = minimum and maximum melt pathways that yield misfit values <2 times minimum misfit; dotted grey lines = adiabatic gradients corresponding to loci of intersection between solidus and melt path (Shorttle et al., 2014). Note that best fitting potential temperature (T_p) in Figure 7G cannot be calculated since all samples equilibrated below the anhydrous solidus. Black symbol shows equilibration uncertainty.

PF2016 geochemical modelling and isostatic calculations of uplift (Figure 7). We estimate that volcanic rocks in the Forties-Piper region (centre of the MNSH) were generated above mantle with a potential temperature (T_p) of 1275–1400°C and a lithosphere thickness (L_t) of 40–60 km (Figure 7b–d). In contrast, volcanic rocks in the Scanian region (margin of the MNSH), were generated above colder (1260–1370°C) mantle and thicker (70–100 km) lithosphere (Figure 7e–g), suggesting that the lithosphere thickened towards the margin of the North Sea rift system. In both regions, it is useful to compare our results to the average values of potential temperatures calculated for a global dataset along the mid-oceanic ridge (MOR) system using the INVMEL and PF2016 models – the average values are 1316°C and 1371°C, respectively (Ball, 2020). Assuming that these MOR values represent estimates of ambient mantle temperatures, our results suggest that at the time of formation, the North Sea generally had a thin lithosphere (60 km) underlain by an ambient to moderately cool mantle. Calculated values of isostatic uplift with estimated initial lithosphere thickness (a_o) of 120 km and $0 > \Delta T > -115$°C are 0.3–0.65 km for the MNSH region (Figure 7; Equation 4). Alternatively, Brodie and White (1995) proposed an empirical relationship to estimate uplift from the amount of denudation that results from both regional uplift and isostatic compensation. Published estimates of the amount of denudation from the MNSH region range from 0.3 to 1.5 km (Husmo et al., 2002; Japsen et al., 2007; Table 2; see Section 2.2). Assuming the density of the asthenosphere is 3.2 g/cm^3 and the density of the overburden is 2.0–2.4 g/cm^3, this empirical relationship (Brodie & White, 1995) gives an estimated uplift of 0.1–0.6 km for the MNSH, which is consistent with the amount of uplift derived from our isostatic estimates (Figure 7).

In applying the BQART model, maximum catchment relief, *R*, is assigned a triangular distribution with the range of values constrained by published studies for each source region and our isostatic uplift estimates for the MNSH, as summarised above (Table 2). The complicated palaeotopographic evolution of southern Norway indicates significant uncertainties in *R* for the Norwegian Landmass and is reflected in the range of 1–3 km, with the most-likely estimate of 1.2 km suggested by thermochronological modelling studies (Gabrielsen et al., 2010). *R* is poorly constrained for the Shetland Platform, but we tentatively estimate it to be no higher than the Norwegian Landmass on the conjugate rift margin, with a range of 0.5–1.5 km and mode of 1.0 km. We assign a range of 0.1–0.6 km and a most-likely estimate of 0.3 km for *R* of the Mid-North Sea High, using constraints from our modelled isostatic uplift estimates (Figure 7), and estimated relief from the amount of denudation (Table 2; Husmo et al., 2002; Japsen et al., 2007; Underhill & Partington, 1993).

There are insufficient data on the area and thickness of eroded units to apply the geometrical reconstruction method to the Norwegian Landmass and Shetland Platform source area. In applying this method to the Mid-North Sea High, catchment area, *A*, is assigned a normal distribution with the same input parameters as in the BQART method (Table 2). The thickness of exhumed mudstone-dominated Lower Jurassic and sandstone-dominated Triassic strata are assigned a triangular distribution with a range of 0.3–1.5 km and most-likely estimate of 0.7 km, based on estimates derived from stratigraphic constraints (Husmo et al., 2002), and integrated sonic velocity, vitrinite reflectance and AFT data (Japsen et al., 2007; Table 2). Bulk-density values of 2.0–2.4 g/cm^3, derived from sediment compaction curves (e.g., Sclater & Christie, 1980), are used to convert sediment volume to mass. The duration of exhumation is assigned a uniform distribution with a range of 8–10 Myr (Table 2; Underhill & Partington, 1993, 1994).

In both methods, the percentage of the sediment budget from the Mid-North Sea High discharged northwards into the Brent Delta system is assigned a triangular distribution with a most-likely value of 20% and range of 10%–30%, based on palaeographic reconstructions of inferred drainage outlets that fed adjacent major delta complexes (Figure 2b; Ziegler, 1990). The remaining 70%–90% of sediment derived from the Mid-North Sea High is interpreted to have been routed northwestwards into the Faroes-Shetland Basin, southwards into the South Permian Basin, eastwards into the Egersund Basin and southeastwards into a depocentre in present-day northern Germany (Figure 2a).

6 | RESULTS

6.1 | Depositional-sink sediment budget

The median (P50) and range (P10-P90) of estimates of net-depositional sediment volumes for genetic sequences J22, J24, J26, and J32 are 660 km^3 (400–930 km^3), 1800 km^3 (1470–2130 km^3), 1490 km^3 (1210–1790 km^3), and 3570 km^3 (2850–4340 km^3), respectively (Table 3, Figure 8a). These values sum to a median cumulative net-depositional sediment volume of 7510 km^3 for the total duration (8.1 Myr) of deposition of the Brent Delta, with a P10-P90 range of 5940–9190 km^3 (Table 3; Figure 8b). Similarly, the median (P50) and range (P10-P90) of estimates for the net-depositional sediment mass for genetic sequences J22, J24, J26 and J32 are 1.7×10^{12} t ($1.0–2.3\times10^{12}$ t), 4.5×10^{12} t ($3.6–5.3\times10^{12}$ t), 3.8×10^{12} t ($3.1–4.5\times10^{12}$ t), and 9×10^{12} t ($7.1–10.8\times10^{12}$ t), respectively, giving a cumulative net-depositional sediment

TABLE 3 Depositional sink sediment budget for the present-day extent of the Brent Delta sediment routing system.

Stratigraphic unit (age)	Duration (Myr)	Net-depositional sediment volume ($\times10^3$ km^3)			Net-depositional sediment mass ($\times10^{12}$ t)			Net-depositional sediment budget (Mt/year)		
		P10	P50	P90	P10	P50	P90	P10	P50	P90
Genetic sequence J22	3.9	0.40	0.66	0.93	0.99	1.65	2.31	0.24	0.43	0.69
(174.2–170.3 Ma)										
Genetic sequence J24	1.1	1.47	1.79	2.13	3.64	4.46	5.31	1.83	3.22	6.79
(170.3–169.2 Ma)										
Genetic sequence J26	0.9	1.21	1.49	1.79	3.05	3.78	4.51	1.58	3.09	6.72
(169.2–168.3 Ma)										
Genetic sequence J32	2.2	2.85	3.57	4.34	7.12	8.97	10.8	2.54	4.07	8.04
(168.3–166.1 Ma)										
Total (J22-J32)	**8.1**	**5.94**	**7.51**	**9.19**	**14.8**	**18.9**	**23**	**1.96**	**2.33**	**2.78**

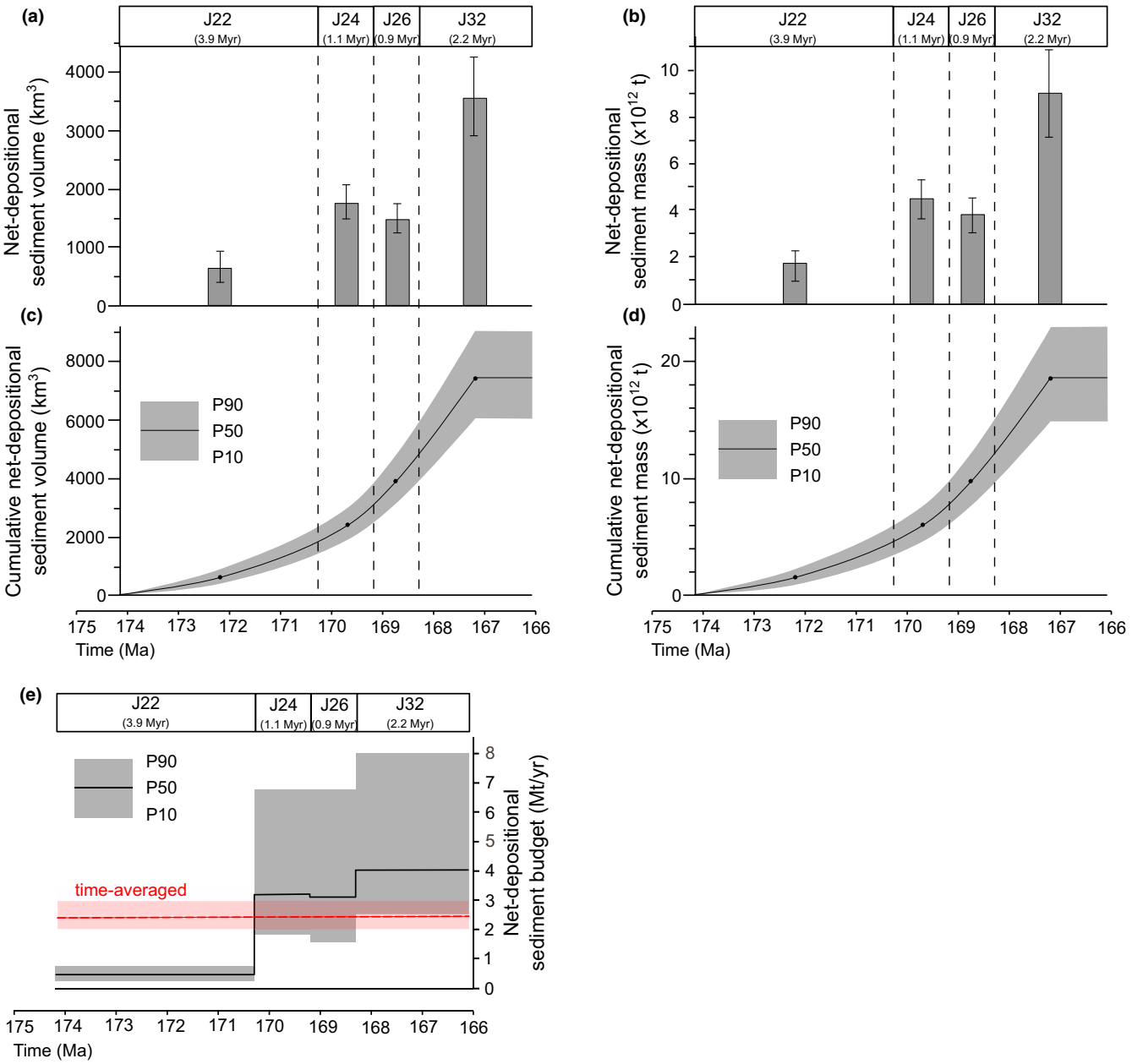

FIGURE 8 Summary of net-depositional sediment budget for the four genetic sequences of the Brent Delta sediment routing system deposits (Figure 4). For each plot, genetic sequences are shown from oldest (J22, left) to youngest (J32, right). (a) Net-depositional sediment volume; (b) cumulative net-depositional sediment volume; (c) net-depositional sediment mass; (d) cumulative net-depositional sediment mass; and (e) net-depositional sediment budget. In Figure 8a and b, grey bars show the median (P50) value and vertical black lines show the 10th to 90th percentile range (P10-P90). In Figure 8c–e, black lines shows the median (P50) value and grey shading shows the 10th to 90th percentile range (P10-P90). In Figure 8e, the time-averaged sediment budget for the entire Brent Delta system is shown as a red dashed line.

mass of 18.9×10^{12} t ($14.8–23\times10^{12}$ t) for the entire Brent Delta (Table 3; Figure 8c,d). The temporal trends in net-depositional sediment volume and mass are similar (Figure 8a–d).

Although there is significant uncertainty in the estimated net-depositional sediment mass budgets, sediment accumulation rate generally increased through time, based on the median (P50) estimates (Table 3; Figure 8e). During J22, the net-depositional sediment budget was relatively low with a median estimate of 0.43 Mt/year and a P10-P90 range of 0.24–0.69 Mt/year. From J22 to J24, the median (P50) estimates of the net-depositional sediment budget increased by nearly a factor of eight, to 3.2 Mt/year, with a P10-P90 range of 1.8–6.8 Mt/year and, significantly, no overlap in the range of uncertainty between J22 and J24 estimates. Estimated net-depositional sediment budget shows a large overlap in range of uncertainty between J24 to J26, with a median estimate of 3.1 Mt/year

and P10-P90 range of 1.6–6.7 Mt/year for genetic sequence J26. From J26 to J32, comparison of median estimates suggests a 32% increase in net-depositional sediment budget to 4.1 Mt/year, with a P10-P90 range of 2.5–8.0 Mt/year during J32, although the large overlap in the range of uncertainty suggests net-depositional sediment budget may have remained constant from J24 through J32 (Figure 8e). For the total duration of Brent Delta deposition, the median, time-averaged net-depositional sediment budget was 2.3 Mt/year, with a P10-P90 range of 2.0–2.8 Mt/year (Table 3; Figure 8e).

Variation in estimates for the net-depositional sediment budget are principally derived from uncertainties in the absolute age duration and net-depositional sediment volume (i.e., mapped area of the depositional sink and thickness of the genetic sequence), with uncertainty in the bulk-density parameter used in converting sediment volume to mass contributing little (<5% for all genetic sequences) to such variation. However, the relative contribution of each input parameter to the range of uncertainty differs for each genetic sequence (Figure 9a–d). For genetic sequence J22, uncertainty in the estimated budget is principally associated with the thickness (56%), possibly due to the generally thin (<60 m) and patchy distribution of this unit (Figure 9a). In contrast, uncertainties in the estimated budget for the younger genetic sequences derive predominantly from the age duration (genetic sequence J24–82%, genetic sequence J26–62%, and genetic sequence J32–84%) (Figure 9b–d). Similarly, for the entire Brent Delta system, uncertainty in the total time-averaged net-depositional sediment budget is principally associated with the absolute age duration (51%), but with significant contributions from the total thickness (23%) and mapped area of the depositional sink (22%; Figure 9e).

6.2 | Source-area sediment budget

The BQART-derived estimated sediment budget supplied from the Norwegian Landmass ranged from 5.0 Mt/yr (P10) to 14.1 Mt/year (P90) with a median (P50) estimate of 8.5 Mt/year (Table 4; Figure 10). The Shetland Platform contributed an estimated sediment budget of 2.3 Mt/year (P10) to 5.6 Mt/year (P90) (Table 4; Figure 10). The median sediment budget estimate for the Shetland Platform (3.7 Mt/year) is 56% less than the comparable estimate for the Norwegian Landmass (8.5 Mt/year), largely influenced by the smaller area of the Shetland Platform catchment (Shetland Platform catchment area is 74% less than that of the Norwegian Landmass catchment area), although this effect is partially offset by differences in bedrock lithology. The median BQART-derived estimate of sediment supplied by the Mid-North Sea High to the Brent Delta sediment routing system is 5.4 Mt/year, with a range of 2.8 Mt/year (P10) to 9.4 Mt/year (P90) (Table 4; Figure 10). This median estimate (5.4 Mt/year) is less than the estimated median contribution from the Norwegian Landmass (8.6 Mt/year), potentially suggesting that the Norwegian Landmass may have been a more important source region during the Middle Jurassic. The total sediment budget derived from the three source regions is estimated to be 17.4 Mt/year with a P10-P90 range of 13.9–23 Mt/year (Table 4).

The estimated sediment supplied by the Mid-North Sea High to the Brent Delta sediment routing system using the geometrical reconstruction method ranges from 4.8 Mt/year (P10) to 14.9 Mt/year (P90) with a median estimate of 8.7 Mt/year (Table 4; Figure 10). Sediment budget estimates derived from this method are consistent with, but generally higher than, the estimates derived from the

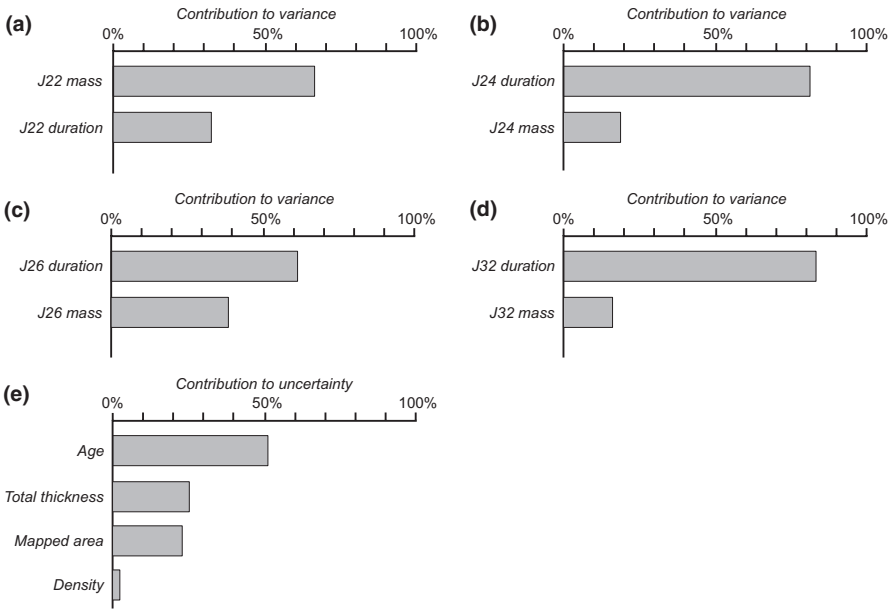

FIGURE 9 Plots showing the sensitivity to input-parameter values of net-depositional sediment budget estimates for the four genetic sequences of the Brent Delta sediment routing system deposits (Figure 4): (a) genetic sequence J22; (b) genetic sequence J24; (c) genetic sequence J26; (d) genetic sequence J32; and (e) entire Brent Delta system.

TABLE 4 Source-area sediment budget for the Brent Delta sediment routing system. The BQART model is applied to all three source regions, while a simple geometrical restoration model is also applied to the Mid-North Sea High. The total sediment budget from the three source regions is the sum of the BQART-derived estimates. Percentage contribution of sediment budget from each source area is based on the median (P50) values of the BQART-derived estimates.

Source area	Source-area sediment budget (Mt/year)			Contribution to total sediment budget
	P10	P50	P90	
Norwegian Landmass (BQART model)	5.0	8.5	14.1	49%
Shetland Platform (BQART model)	2.3	3.7	5.6	21%
Mid-North Sea High (BQART model)	2.8	5.4	9.4	30%
Mid-North Sea High (geometrical reconstruction model)	4.8	8.7	14.9	-
Total sediment budget (BQART)	**13.9**	**17.4**	**23.0**	**100%**

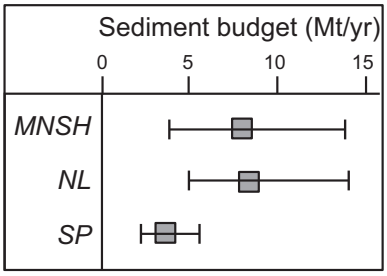

FIGURE 10 Plot showing comparison of sediment budgets estimated for the three sediment source regions of the Brent Delta sediment routing system, the Mid-North Sea High (MNSH), Norwegian Landmass (NL), and Shetland Platform (SP) (Figures 2, 3). Estimates are generated using the BQART model for MNSH, NL and SP, and using a simple geometrical reconstruction model for the MNSH. Grey squares show the median (P50) value and horizontal black lines show the 10th to 90th percentile range (P10-P90).

BQART model. Higher estimates from the geometrical reconstruction method may be explained by pre-uplift thickness variation in the eroded Lower Jurassic and Triassic units (a spherical dome geometry assumes constant thickness), smaller thickness of eroded sediments, and/or longer duration of exhumation (Figure 10; Table 4).

Uncertainty in the BQART-derived sediment budget estimates for all three source regions is principally associated with relief, R (42%, 40% and 51% in the Norwegian Landmass, Shetland Platform and Mid-North Sea High, respectively; Figure 11a–c). Other catchment-controlled parameters (A, L) also contribute significantly to uncertainty in the sediment budget estimates; 17%, 25% and 14% for A, and 28%, 19% and 5% for L in the sediment budget estimates for the Norwegian Landmass, Shetland Platform and Mid-North Sea High, respectively (Figure 11a–c). In contrast, palaeoclimate-controlled parameters (T, r) contribute less, <17% in total, to uncertainty in sediment

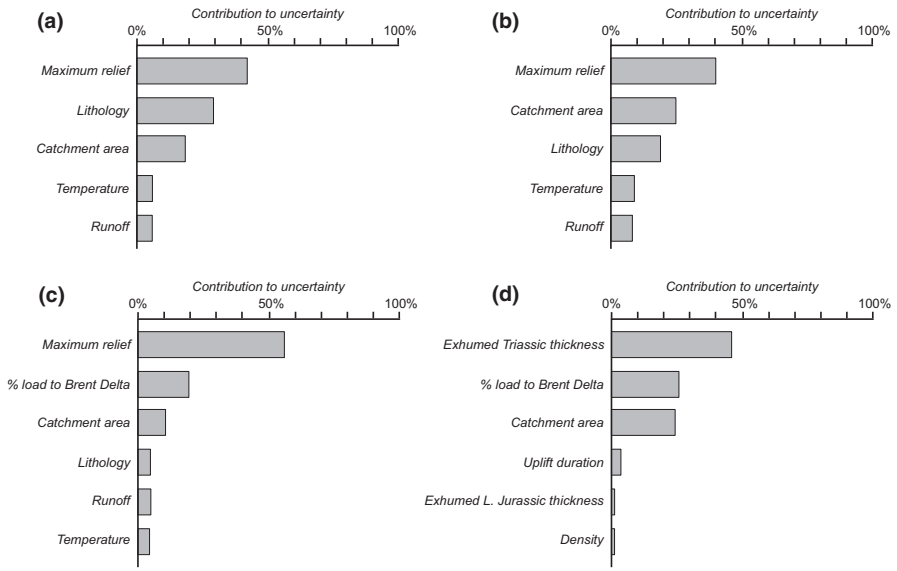

FIGURE 11 Plots showing the sensitivity to input-parameter values of sediment budget estimates from the three sediment source regions of the Brent Delta sediment routing system: (a) Norwegian Landmass using the BQART model; (b) Shetland Platform using the BQART model; (c) Mid-North Sea High using the BQART model; (d) Mid-North Sea High using the geometrical reconstruction method.

budget estimates for each of the three source regions (Figure 11a–c). Uncertainty in the sediment budget estimate derived from the geometrical reconstruction method is principally associated with the thickness of exhumed Lower Jurassic and Triassic strata (44%), with a significant contribution from the catchment area, *A* (26%) (Figure 11d). The duration of exhumation and sediment bulk-density each contribute little (<5%) to uncertainty in the sediment budget (Figure 11d). The results of both methods applied to the Mid-North Sea High are sensitive to the proportion of the total sediment budget that was fed northwards to the Brent Delta system, which contributes significantly (21%–27%) to uncertainty in the sediment budget estimates (Figure 11c,d).

6.3 | Relative contribution of different source regions

The relative contribution of different sediment source regions can be estimated independently in the depositional sink using sandstone provenance data. Morton (1992) documents detrital garnet compositional suites from Brent Group sandstones that can be related to the Shetland Platform, Norwegian Landmass and Mid-North Sea High source regions (respectively the "A-dominated", "B-dominated" and "Cde-dominated" suites of Morton, 1992). Although detrital garnet compositional data were collected from only 15 wells, the sampled wells are distributed across the Brent Province. The relative proportions of the detrital garnet compositional suites for each of the four genetic sequences of the Brent Delta sediment routing system (J22, J24, J26, and J32) is used to infer the predominant sediment source region during each time interval (Figure 12).

Detrital garnet compositional data indicate that the Broom and Oseberg formations (genetic sequence J22; Figures 3a and 4) were supplied predominantly from the Shetland Platform and Norwegian Landmass source regions, respectively (Figure 12a). The Rannoch, Etive and lower Ness formations (genetic sequence J24; Figures 3b and 4) were supplied predominantly from the Norwegian Landmass (62%), with smaller contributions from the Mid-North Sea High (28%) and Shetland Platform (10%) (Figure 12b). The middle and upper Ness formations (genetic sequence J26; Figures 3c and 4) were supplied mainly from the Mid-North Sea High (40%), with significant contributions from the Norwegian Landmass (38%) and Shetland Platform (22%) (Figure 12c), whereas the Tarbert Formation (sequece J32; Figures 3d and 4) was supplied mainly from the Norwegian Landmass (48%) and Shetland Platform (30%) (Figure 12d). For the overall duration of Brent Delta deposition (8.1 Myr), the detrital garnet compositional data weighted by the net-depositional sediment budget for each of the four stratigraphic units, suggest that the median (P50) relative contribution to sediment supply from the Norwegian Landmass, Shetland Platform and Mid-North Sea High were approximately 46%, 28% and 26%, respectively, based on the median estimates (Figure 13).

The sediment budgets of the three different sediment source regions are estimated by the BQART model over the duration of the Brent Delta sediment routing system (Figure 10). The median relative contributions of the Norwegian Landmass, Shetland Platform and Mid-North Sea High, based on BQART-derived sediment budget estimates, were 49%, 21% and 30%, respectively (Figure 13; Table 4). These relative contributions are consistent with those derived independently from detrital garnet compositional data (Morton, 1992), within the large ranges of uncertainty associated with both methods (Figure 13), although the magnitude of estimated sediment budgets for the source area and mapped depositional sink differ significantly. The broad consistency in results for the two methods provides confidence in the relative contributions of different sediment source regions.

7 | DISCUSSION

7.1 | Potential drivers of sediment budget variation

Regional-scale, long-term variations in sediment supply are typically driven by perturbations in climatic (e.g., temperature, precipitation, water discharge) and/or tectonic (e.g., catchment reorganisation, uplift rate, fault movement) boundary conditions (Allen et al., 2013; Helland-Hansen et al., 2016; Hinderer, 2012; Lyster et al., 2020; Romans et al., 2016). Such variations in sediment budget for the Brent Delta sediment routing system are discussed below within the tectono-climatic context of the Northern North Sea area.

Regional palaeoclimate proxies (summarised in Section 2.3) indicate that there was no major shift in climate during the Middle Jurassic of the Northern North Sea (Prokoph et al., 2008; Sellwood & Valdes, 2006). As previously outlined, the long-term relative contribution to sediment supply from the three source regions derived from depositional sink-focused detrital garnet data are broadly consistent with those independently derived from source area-focused BQART model (Figure 13). This consistency suggests that sediment supply signals may have propagated from the erosional source regions to the depositional sink, with little apparent buffering in the transfer zones (Romans et al., 2016). Assuming this to be the case, the relative

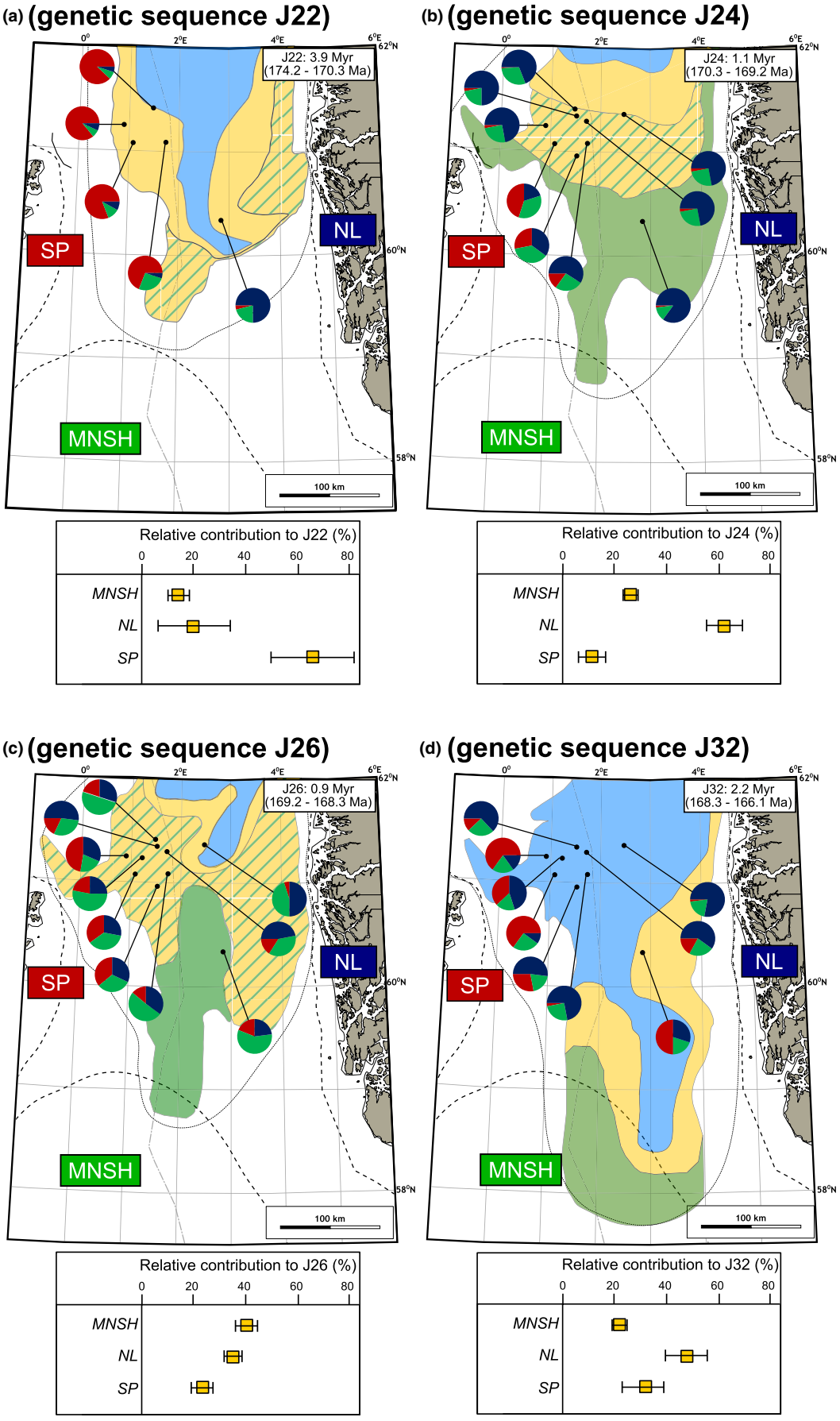

contribution from source regions to each of the four stratigraphic units (Figure 12), provides insights to the possible external drivers of spatial and temporal variations in sediment budget. Figure 14 summarises variations in sediment budget for the Brent Delta system, linked to stratigraphic architecture, relative contribution from source regions, climate, eustatic sea-level change, and possible tectonic drivers in the source regions and depositional sink.

During the Aalenian (genetic sequence J22), a relatively low sediment influx was delivered to the Brent Delta sediment routing system (median estimate of 0.43 Mt/year), predominantly from the Shetland Platform and Norwegian Landmass (Figures 9e, 12a and 14), which were respectively the western and eastern degraded margins of an antecedent Permian – Early Triassic rift system (Deng et al., 2017; Phillips et al., 2019; Zanella & Coward, 2003) that supplied minor progradational wedges of coarse-grained fluvial-tidal sediments of the Broom and Oseberg formations (Figures 3a, 5 and 14; Husmo et al., 2002). The influx of coarse-grained sediment implies renewed uplift of the inherited Triassic rift shoulders, (e.g., Helland-Hansen et al., 1992; Steel, 1993). The base of genetic sequence J22 is marked by a regionally extensive intra-Aalenian unconformity ("Mid-Cimmerian Unconformity") that truncates Lower Jurassic marine shales and older Triassic sedimentary rocks and records the initiation of uplift and volcanism in the Mid-North Sea High region (Husmo et al., 2002; Steel, 1993; Underhill & Partington, 1993, 1994; Ziegler, 1990).

Subsequently, there was a pronounced increase in the net-depositional sediment budget (by a factor of eight, based on median estimates) from Aalenian (genetic sequence J22) to Early Bajocian (genetic sequence J24), which coincides with the main northward progradation of the wave-dominated Brent Delta (Figures 3b, 5, 9e and 14). When catchments are perturbed by external tectonic or climatic forcing, there may be a delayed response before environmental signals propagate from net-erosional source regions to net-depositional sinks (Duller et al., 2019; Gong et al., 2018; Li et al., 2018; Sharman et al., 2019; Sømme & Jackson, 2013; Whittaker et al., 2010) – this delayed response may represent millions of years (e.g., Whittaker et al., 2010). The time lag between initiation of the intra-Aalenian unconformity, which represents the tectonic perturbation during the Aalenian (genetic sequence J22; *c.* 174 Ma; Underhill & Partington, 1993, 1994), and the subsequent increase in sediment influx in the Early Bajocian (genetic sequence J24; *c.* 170–169 Ma) is interpreted to reflect a response time of 4 Myr for the Brent Delta sediment routing system. Increased sediment supply in the Early Bajocian was primarily driven by increased relative contributions from the Norwegian Landmass and Mid-North Sea High (Figures 11b and 13). Greater sediment flux from these two source regions in the Early Bajocian is consistent with significant increases in the catchment relief of the Mid-North Sea High (Quirie et al., 2020; Underhill & Partington, 1993, 1994) and of the Norwegian Landmass (Gabrielsen et al., 2010; Ksienzyk et al., 2014; Medvedev & Hartz, 2015), assuming the area of the catchments feeding the system did not change significantly. The relief of the Shetland Platform, although poorly constrained in published literature, is not inferred to have increased significantly relative to other source regions in the Early Bajocian.

Estimated net-depositional sediment budgets remained high throughout the Bajocian and Bathonian, from genetic sequence J24 to genetic sequences J26 and J32 (Figures 7e and 14). However, the dominant sediment source region switched from the Mid-North Sea High during the Late Bajocian (genetic sequence J26) to the Norwegian Landmass and Shetland Platform during the Bathonian (genetic sequence J32; Figure 12c,d). We infer that the greatest relative contribution from the Mid-North Sea High during the Late Bajocian (genetic sequence J26; *c.* 169–168 Ma) represents a delayed response of approximately 2 Myr to the greatest denudation of this source region during or after Late Aalenian peak uplift (*c.* 171–170 Ma; Quirie et al., 2020). The change in dominant source region in the Bathonian is consistent with uplift and denudation of the eastern and western margins (Norwegian Landmass and Shetland Platform, respectively) of a rift system initiated just before or during the Bathonian (Davies et al., 2000; Folkestad et al., 2014; Helland-Hansen et al., 1992; Figure 14). In this context, and given the consistently high sediment supply, the shift in stratigraphic architecture from progradation to aggradation in the Bajocian (genetic sequences J24 and J26) to retrogradation in the Bathonian (genetic sequence J32; Figures 3b–d, 5 and 14; Hampson et al., 2004; Husmo et al., 2002) is consistent with increased accommodation generation in the basin due to active rifting, potentially enhanced by eustatic sea level rise (Folkestad et al., 2014; Haq, 2018; Figure 14).

FIGURE 12 Relative contribution of source areas to genetic sequences of the Brent Delta sediment routing system (Figure 4), estimated from the relative proportion of detrital garnet compositional suites of Morton (1992): (a) genetic sequence J22; (b) genetic sequence J24; (c) genetic sequence J26; and (d) genetic sequence J32. Source areas are MNSH (Mid-North Sea High), NL (Norwegian Landmass) and SP (Shetland Platform).

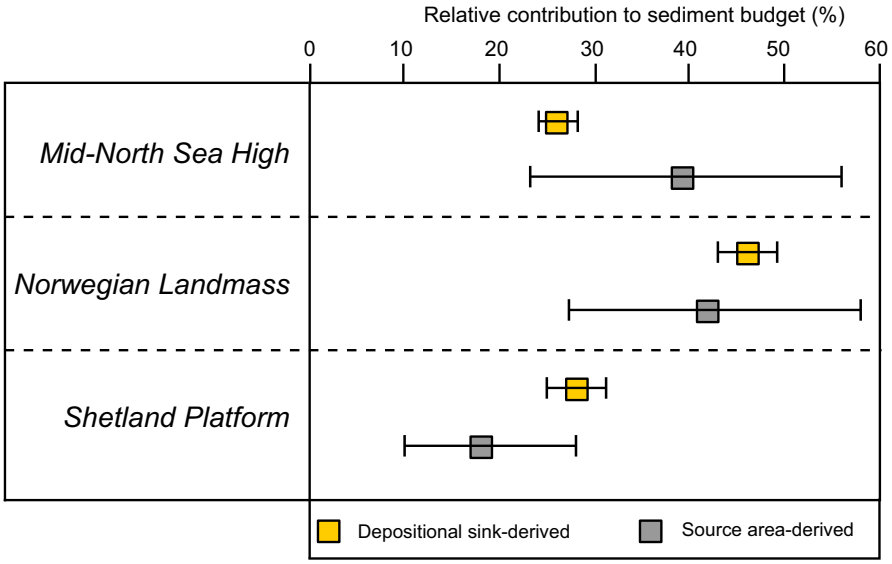

FIGURE 13 Relative contribution of the Mid-North Sea High, Norwegian Landmass, and Shetland Platform over the entire duration of Brent Delta deposition. The relative contribution derived from the source areas using the BQART method (grey squares) are comparable to, and overlap with, those derived independently from detrital garnet compositional data (yellow squares) of Morton (1992), within large uncertainty ranges associated with both methods.

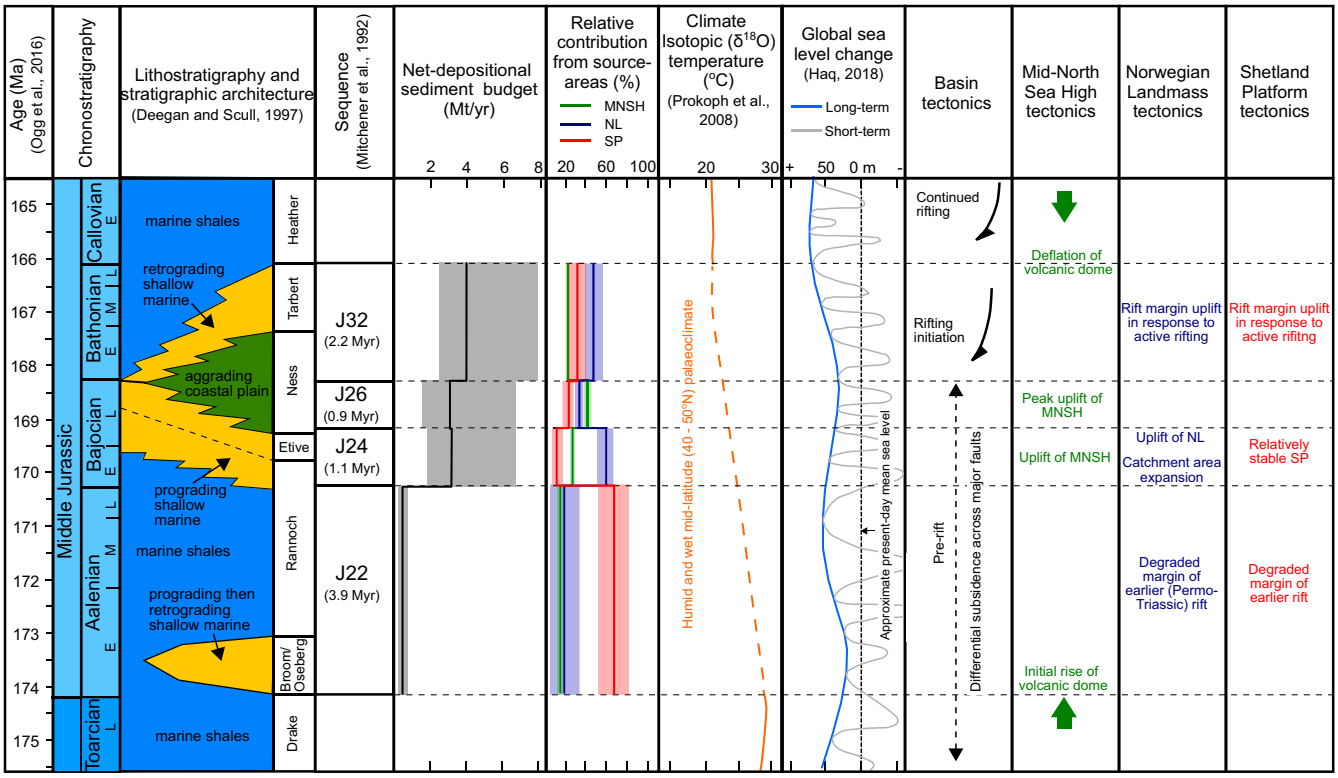

FIGURE 14 Summary of Aalenian (genetic sequence J22) to Bathonian (genetic sequence J32) sediment budgets for the Brent Delta sediment routing system, linked to stratigraphic architecture, relative contribution from source regions, climate, eustatic sea-level change, and possible tectonic drivers in source regions and depositional sink (see text for explanation).

7.2 | Discrepancy between source-area and depositional-sink sediment budget

Recent studies have shown that applying the BQART model to source regions can provide reasonable predictions of sediment flux that are consistent, within one order of magnitude, when compared to estimated sediment budget in the downsystem stratigraphic record in sub-modern (Watkins et al., 2018) and ancient depositional sinks (Brewer et al., 2020; Gilmullina et al., 2022; Lyster et al., 2020; Zhang et al., 2018). However, our analysis of the Brent Delta system suggests that the mapped net-depositional sediment budget (2.0–2.8 Mt/year, median

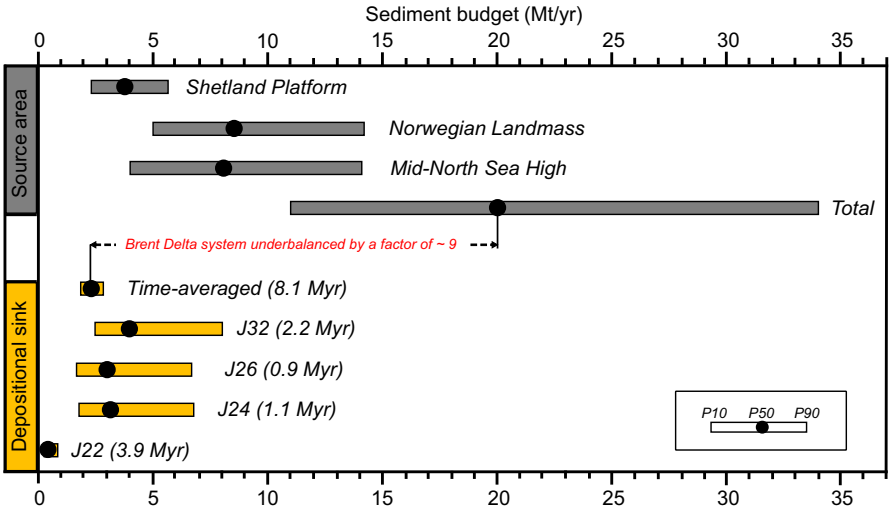

FIGURE 15 Comparison of the estimates of the total BQART-predicted sediment budget from the three source regions (grey shade; median P50 value = 20 Mt/year), and mapped depositional-sink sediment budget (yellow shade; median P50 value = 2.3 Mt/year) of the Brent Delta sediment routing system. Time-averaged depositional sink sediment budget is approximately one order of magnitude less than the total BQART-predicted sediment budget from the source areas.

estimate: 2.3 Mt/year) is about an order of magnitude less than the total BQART-predicted sediment budget from the three source regions (13.9–23.0 Mt/year, median estimate: 17.4 Mt/year; Figure 15).

We evaluated the possible sources of error and uncertainty in our input data to generate a probabilistic range of sediment budget estimates, and assessed the sensitivity of each parameter using Monte Carlo simulation (Figures 8 and 11). The greatest contribution to uncertainties in the BQART-predicted source-area sediment budget estimates (Figure 10) are from the maximum relief (R), catchment area (A), and catchment-averaged lithology (L) (Figure 11), reflecting the inherent challenges associated with reconstructing palaeocatchment characteristics of ancient sediment routing systems (Brewer et al., 2020; Nyberg et al., 2021). Nyberg et al. (2021) further noted that L is a qualitative estimate with quantitative thresholds that may not be proportional to the observed variability in lithologies within a catchment and suggests applying an uncertainty range of at least a factor of two. More uncertainties in palaeocatchment characteristics reside in the: (i) proportion of predicted sediment budget from the Mid-North Sea High funnelled through the Brent Delta system (10%–30%, Figures 2b and 11), and (ii) position of drainage divides which constrain catchment areas (e.g., in the Shetland Platform and Norwegian Landmass; Figure 2b), for which we assigned a plausible range of uncertainty to be 20% around the estimated (median) catchment area. It is unlikely that a smaller area for any of the source regions fed the Brent Delta system, based on published palaeogeographical reconstructions (Figure 2b; Torsvik et al., 2002; Underhill & Partington, 1993; Ziegler, 1990).

The BQART-predicted sediment budget is less sensitive to uncertainties in runoff (r) and catchment-averaged temperature (T), especially in warm and humid climates, as is the case in the study area (Figure 10; Lyster et al., 2020; Nyberg et al., 2021). Although the model accounts for the proportion of sediment stored within catchments and/or transfer-zone sinks (T_E in Equation 3; Syvitski & Milliman, 2007), this proportion is often challenging to quantify in ancient sediment routing systems and is not accounted for in our BQART analysis, since it is only likely to be significant in large (catchment area $>10^6$ km^2, transfer zone length >300 km) sediment routing systems (e.g., Lyster et al., 2020; Zhang et al., 2018). Additionally, the BQART model neither accounts for bedload sediment transport (it only predicts suspended sediment load), nor low-frequency, high-magnitude discharge events (e.g., earthquake- and storm-triggered landslides), both of which may be volumetrically significant over geological timescales (Helland-Hansen et al., 2016; Pratt-Sitaula et al., 2007; Turowski et al., 2010; Watkins et al., 2020). A further question is how the short-term (10^1 year) measurements of sediment flux on which the BQART model was developed translate to long-term ($>10^6$ years) fluxes estimated within an ancient system (Paola et al., 2018; Sadler, 1999). In practice, not accounting for certain uncertainties (e.g., sediment storage) may lead to overprediction of sediment budget, which may be offset by our inability to constrain some other uncertainties (e.g., bedload contribution to sediment flux).

For the mapped depositional sink, the major uncertainty in net-depositional sediment budget is the absolute ages of the surfaces bounding genetic sequences J22, J24, J26 and J32 (Gradstein et al., 2012; Ogg et al., 2016), which determines the duration of each genetic sequence – a shorter duration would increase the estimated sediment budget (Figure 8). Further uncertainties lie in the mass of sediments eroded after Middle Jurassic deposition. By extrapolating isopach contour trends beyond the mapped extent of preserved Brent Delta deposits to the inferred extent of deposition at the basin margins prior to Late Jurassic erosion (Figures 3 and 6; Husmo et al., 2002), a potential additional sediment mass of up to 40% can be added to the net-depositional sediment budget shown in Figure 8b,d.

Additionally, preserved sediment thickness, especially for genetic sequence J32, may also have been underestimated locally as later uplift during the Late Jurassic and Early Cretaceous resulted in fault block rotation and erosion at the Base Cretaceous Unconformity (e.g., in the Snorre footwall area; Davies et al., 2000), but this uncertainty is non-systematic and does not account for a significant proportion (<10%) of the sediment budget.

Despite these uncertainties, the order-of-magnitude discrepancy between estimated sediment budgets for the erosional source areas and net-depositional sink (Figure 15) implies that most (>75%) of the sediment budget supplied to the Brent Delta sediment routing system is "missing" from the mapped depositional sink. We attribute this discrepancy in sediment budgets to net-export of sediment beyond the limit of the mapped depositional sink by wave-generated longshore currents and/or sediment gravity flows down-dip to the basin floor, as discussed below. The "missing" sediments are interpreted to have been transported westward into the Faroe-Shetland Basin (Figure 2a) by longshore currents or northward into the western Møre Basin (Figure 2a) by sediment gravity flows, as explored further below (Figure 16). The imbalance of sediment budget between erosional source and depositional sink, even in well-studied systems like the Brent Delta, has significant implications for the application of mass-balance frameworks in ancient sediment routing systems and directly suggests that the documented stratigraphic extent of such systems, even when well-studied, is incomplete (c.f. Allen, 2017; Michael et al., 2014).

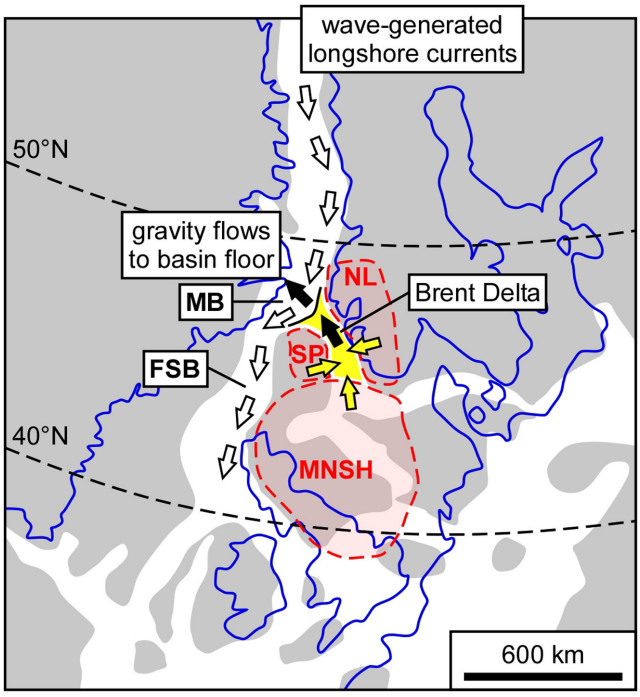

FIGURE 16 Unrestored Middle Jurassic palaeogeographical reconstruction of the North Sea (Figure 2a) illustrating interpreted dispersal of excess sediment supplied by the Brent Delta sediment routing system. This sediment was dispersed via along-shore transport by wave-generated currents and down-dip transport to the basin floor by gravity flows. Potential sinks for the excess sediment include the Faroes-Shetland Basin (FSB) and Møre Basin (MB).

Abundant wave ripples and hummocky cross-stratification in the thick (100 m) prograding shoreface successions of the Brent Delta (Rannoch Formation, genetic sequence J24) indicate a storm wave-dominated shelf with abundant sand supply (Figure 5; Hampson et al., 2004; Husmo et al., 2002; Supplementary Material), which is consistent with strong along-shore wave-generated currents, and possibly other ocean currents, redistributing sediments in the marine depositional sink. The relative abundance of shoreface-shelf sandstones sourced from the Norwegian Landmass relative to the Shetland Platform (Rannoch and Etive formations in Figure 12b; Morton, 1992) implies that longshore currents were directed southwestward into the Faroe-Shetland Basin (Figure 16). This interpretation is supported by the occurrence of shallow-marine sandstones derived from the northeast and northwest along the northeastern margin of the Møre Basin (Morton et al., 2009). Analogues of storm wave-generated currents and wave-enhanced gravity flows redistributing large sediment masses (typically of mud) for long distances abound in modern systems (Addington et al., 2007; Eyal et al., 2021; Friedrichs & Wright, 2004; Kuehl et al., 2004; Macquaker et al., 2010; Manighetti & Carter, 1999; Traykovski et al., 2007), and have also been documented in ancient systems (Ghadeer & Macquaker, 2011; Plint, 2014). Hyperpycnal flows during river flooding events, which can transport substantial mass of sediments to marine depositional sinks (Mulder et al., 2003), also likely played a role in redistributing sediments in the Brent Delta system (Slater et al., 2017). We speculate that these and other sediment gravity flows may have potentially transported sediment into the western Møre Basin, where Jurassic strata occur in deeply buried (at least 6–10 km), rotated fault blocks at the present day (e.g., Brekke et al., 1999; Nirrengarten et al., 2014). These Jurassic strata are not penetrated by wells, but are inferred to comprise deep-marine mudstones (e.g., Brekke et al., 1999). Along well-documented ancient and modern shelf margins, respectively 50%–80% and up to 90% of river-derived sediment is bypassed to the basin floor (Walsh & Nittrouer, 2003; Petter et al., 2013), implying that such sediment bypass can potentially account for the additional sediment supplied by the Brent Delta sediment routing system.

The observations and discussions presented above illustrate the complex dynamic interactions along a

sediment routing system, the modulation of catchment-derived fluvial sediment discharge by marine transport processes in the shoreline-shelf geomorphic segment of the depositional sink, and how these processes can affect sediment budget calculations and mass-balance analyses.

7.3 | Implications for future application of sediment mass-balance analysis

Ancient sediment routing systems with multiple sources and sinks, such as the one studied here, are difficult to fully characterise as erosional source regions are rarely preserved, making it challenging to resolve the extent of individual source regions and their relative contribution to the total sediment budget. Techniques to constrain the age, lithology and distribution of catchment bedrock (e.g., detrital mineral geochronology, bulk-geochemistry; Dickinson & Gehrels, 2010; Sharman et al., 2017; Whitchurch et al., 2011), palaeorelief (e.g., stable isotope palaeoaltimetry, palaeobiology; Fernandes & Roberts, 2021; Rowley, 2007; Sun et al., 2015), and denudation rates (e.g., fission-track thermochronology, cosmogenic isotope analyses; Lupker et al., 2017; Tinker et al., 2008) from the geological record, as well as inverse models to unmix sediment composition into end-member "parent" source regions (Blowick et al., 2019; Lipp et al., 2020, 2021; Sharman & Johnstone, 2017; Weltje & Brommer, 2011) are required to address this challenge.

Similarly, it is often challenging to identify sediment transport pathways (e.g., multiple feeder trunk channels) and fully map the mass of sediments deposited in the associated sinks over the time interval of interest, due to incomplete preservation of the stratigraphic record, limited accuracy in age dating of key isochronous surfaces, and sparse spatial and temporal resolution of geological data (Helland-Hansen et al., 2016; Hinderer, 2012; Sadler, 1981). Where possible, more than one method of quantifying sediment budget should be employed to mitigate the effects of errors and uncertainty specific to one method by cross-validating them, and assess confidence in the results (Brewer et al., 2020).

Most applications of mass-balance frameworks for reconstructing palaeocatchment characteristics and external forcing implicitly assume that the sediment routing system is closed, with the sediment mass supplied by erosional source area(s) being equal to sediment mass in the depositional sink(s) over the time interval of interest (Carvajal & Steel, 2012; Rohais & Rouby, 2020; Sømme & Jackson, 2013; Sømme et al., 2013). However, the extent to which sediment mass-balance is feasible, even in data-rich and structurally-confined depositional sinks, is often not well evaluated, as net-export or net-import of sediment (e.g., by marine transport processes as outlined above) and intrabasinal sediment sourcing are usually not accounted for in these supposedly closed systems. This raises concerns as to how practicable it is to balance erosional and depositional sediment budgets, particularly in leaky or open sediment routing systems, which are significantly more common in the geological record (Gilmullina et al., 2022; Weltje & Brommer, 2011).

Our results demonstrate that a mass-balance framework is useful to evaluate sediment routing and dispersal via mass-balance discrepancies between sediment sources and sinks. Integration of grain-size data could further our understanding of sediment mass-balance (Duller et al., 2010; Reynolds, 2019). By documenting the upsystem calibre of input grains supplied and the downsystem distribution of grain-size fractions, changes in the proportion and rate of downsystem fining of grain-size fractions could be linked to changes in tectonic and/or climatic forcing (Allen et al., 2017; Armitage et al., 2011; Armitage et al., 2015; Michael et al., 2013, 2014; Parsons et al., 2012; Whittaker et al., 2010, 2011), and to lateral sediment export or import (Hampson et al., 2014; Harries et al., 2019). Integration of multiple sedimentary signals, for example through coupling changes in sediment supply and grain-size distribution with changes in sediment composition and provenance, could also provide additional constraints on how sediment routing systems respond to changing forcing in the erosional source regions (Hessler et al., 2017; Sharman et al., 2019), but the effect of grain size-selective transport on compositional variation should be accounted for (Garzanti et al., 2009).

8 | CONCLUSIONS

We have compiled a comprehensive sediment mass-balance budget for the Middle Jurassic (Aalenian – Bathonian) Brent Delta sediment routing system in the Northern North Sea, from the sedimentary basin (depositional sink) to the upstream catchment areas (source regions), using an integrated dataset of published age-constrained stratigraphic schemes, palaeogeographical models and palaeocatchment constraints, provenance data, regional isopach maps, subsurface cores, and well logs. Our approach incorporates a Monte Carlo simulation of the probabilistic range of sediment budget estimates, which accounts for uncertainties in the geologically constrained input parameters, and tests the sensitivity of sediment budget estimates to these input parameters.

The Brent Delta is an ancient wave-dominated sediment routing system consisting of four age-constrained genetic sequences of varying time duration (0.9–3.9 Myr)

that record the initial transverse progradation of basin-margin deltas sourced from the Shetland Platform to the west and Norwegian Landmass to the east (genetic sequence J22), subsequent rapid progradation and aggradation of the delta along the basin axis sourced from the Mid-North Sea High to the south, as well as the western and eastern source regions (genetic sequences J24 and J26), and the final retreat of the delta (sequence 32). Temporal variations in sediment budgets of these genetic sequences within the depositional sink are linked to tectonic perturbations in the three source regions; for example, the pronounced increase in the net-depositional sediment budget from genetic sequence J22 to genetic sequence J24 coincides with rapid progradation of the delta along the basin axis caused by tectonic uplift and increased relief in the Mid-North Sea High and Norwegian Landmass source regions, with a sedimentary response time lag of $>10^6$ years.

The estimated total sediment budget into the Brent Delta sediment routing system from the three source regions was 13.9–23.0 Mt/year, based on the empirical BQART sediment budget prediction model and a simple geometrical reconstruction model. Despite the uncertainties in our estimates, the total sediment budget from all source regions is about an order of magnitude greater than the mapped net-depositional sediment budget in the depositional sink (2.0–2.8 Mt/year). We attribute this marked discrepancy to net-export and redistribution of sediments beyond the limit of the primary depositional sink of the Viking Graben – Horda Platform depocentre of the northern North Sea, probably by wave-generated longshore currents directed southwestward into the Faroe-Shetland Basin and/or by sediment gravity flows into the western Møre Basin. Notwithstanding this order-of-magnitude discrepancy, the relative contributions from each source region estimated from the BQART model are broadly consistent with those independently estimated from published garnet provenance data in the depositional sink.

Our study demonstrates the application of sediment mass-balance methods to ancient sediment routing systems delimited by relatively sparse, low-resolution subsurface geological data, in contrast to higher resolution geological data available for modern sediment routing systems. It however emphasises the need to robustly evaluate the extent to which source region and depositional sink sediment budgets are balanced and whether this is in fact feasible, before extrapolations about palaeocatchment geometries can be made from sediment volumes in the depositional sink. This study further highlights how quantitative mass-balance methods help refine interpretation and/or understanding of external forcing mechanisms on observed stratigraphic architecture and quantifies the potential effects of marine basinal process on sediment budgets, thereby improving predictability in the volume and characteristics of sediments into the depositional sink(s) for resource exploration. Specifically, the study implies that the Faroe-Shetland Basin and/or western Møre Basin contain large Middle Jurassic sediment volumes, potentially including reservoir sandstones, supplied by the Brent Delta sediment routing system. Our work also highlights that the currently documented extent of well-studied sediment routing systems such as the Brent Delta system may not be complete.

ACKNOWLEDGEMENTS

We are grateful for the constructively critical reviews of Christian Haug Eide, John Holbrook, Ron Steel and editorial comments of Cari Johnson. This research was supported by the Petroleum Technology Development Fund of Nigeria through a scholarship grant to ICO (project grant number: PTDF/ED/PHD/OIC/848/16). We thank the British Geological Survey (Nottingham, United Kingdom) and the Norwegian Petroleum Directorate (Stavanger, Norway) for permission to access the subsurface core repositories and well data for this study. We also thank Christopher Brewer, Oliver Jordan (Equinor), Christopher Jackson, Howard Johnson, and members of the Basins Research Group for constructive and encouraging discussions at various stages of this study.

CONFLICT OF INTEREST STATEMENT

There is no conflict of interest.

PEER REVIEW

The peer review history for this article is available at https://www.webofscience.com/api/gateway/wos/peer-review/10.1111/bre.12765.

DATA AVAILABILITY STATEMENT

The data that support the findings of this study are publically available from the sources listed below: – core, offshore UK can be viewed at the National Geological Repository, British Geological Survey (https://www.bgs.ac.uk/geological-data/national-geological-repository/) – wireline logs, offshore UK from the UK National Data Repository, North Sea Transition Authority (https://ndr.nstauthority.co.uk) – core, offshore Norway can be viewed at the Geobank, Norwegian Petroleum Directorate (https://www.npd.no/en/facts/geology/geobank/) – wireline logs, offshore Norway from the Diskos Well Database, Norwegian Petroleum Directorate (https://www.npd.no/en/diskos/wells/) – all other data are taken from publications, which are cited and listed in this paper.

ORCID

Gary J. Hampson https://orcid.org/0000-0003-2047-8469

REFERENCES

Abbink, O., Targarona, J., Brinkhuis, H., & Visscher, H. (2001). Late Jurassic to earliest cretaceous palaeoclimatic evolution of the southern North Sea. *Global and Planetary Change*, *30*, 231–256.

Addington, L. D., Kuehl, S. A., & McNinch, J. E. (2007). Contrasting modes of shelf sediment dispersal off a high-yield river: Waiapu River, New Zealand. *Marine Geology*, *243*, 18–30.

Allen, P. A. (2017). *Sediment routing systems: The fate of sediment from source to sink*. Cambridge University Press.

Allen, P. A., Armitage, J. J., Carter, A., Duller, R. A., Michael, N. A., Sinclair, H. D., Whitchurch, A. L., & Whittaker, A. C. (2013). The Qs problem: Sediment volumetric balance of proximal foreland basin systems. *Sedimentology*, *60*, 102–130.

Allen, P. A., & Heller, P. L. (2011). Dispersal and preservation of tectonically generated alluvial gravels in sedimentary basins. In C. Busby & A. Azor (Eds.), *Tectonics of sedimentary basins: Recent advances* (pp. 111–130). Blackwell.

Allen, P. A., Michael, N. A., D'Arcy, M., Roda Boluda, D. C., Whittaker, A. C., Duller, R. A., & Armitage, J. J. (2017). Fractionation of grain size in terrestrial sediment routing systems. *Basin Research*, *29*, 180–202.

Armitage, J. J., Allen, P. A., Burgess, P. M., Hampson, G. J., Whittaker, A. C., Duller, R. A., & Michael, N. A. (2015). Sediment transport model for the Eocene Escanilla sediment-routing system: Implications for the uniqueness of sequence stratigraphic architectures. *Journal of Sedimentary Research*, *85*, 1510–1524.

Armitage, J. J., Duller, R. A., Whittaker, A. C., & Allen, P. A. (2011). Transformation of tectonic and climatic signals from source to sedimentary archive. *Nature Geoscience*, *4*, 231–235.

Ball, P. (2020). *Global relationships between intraplate magmatism and dynamic topography*. Unpublished PhD thesis. University of Cambridge.

Ball, P. W., White, N. J., Maclennan, J., & Stephenson, S. N. (2021). Global influence of mantle temperature and plate thickness on intraplate volcanism. *Nature Communications*, *12*, 1–13.

Barton, P., & Wood, R. (1984). Tectonic evolution of the North Sea basin: Crustal stretching and subsidence. *Geophysical Journal International*, *79*, 987–1022.

Bhattacharya, J. P., Copeland, P., Lawton, T. F., & Holbrook, J. (2016). Estimation of source area, river paleo-discharge, paleoslope, and sediment budgets of linked deep-time depositional systems and implications for hydrocarbon potential. *Earth-Science Reviews*, *153*, 77–110.

Blowick, A., Haughton, P., Tyrrell, S., Holbrook, J., Chew, D., & Shannon, P. (2019). All mixed up: Pb isotopic constraints on the transit of sands through the Mississippi-Missouri River drainage basin, North America. *Bulletin of the Geological Society of America*, *131*, 1501–1518.

Brekke, H., Dahlgren, S., Nyland, B., & Magnus, C. (1999). The prospectivity of the Vøring and Møre basins on the Norwegian Sea continental margin. In A. J. Fleet & S. A. R. Boldy (Eds.), *Petroleum geology of Northwest Europe: Proceedings of the 5th Petroleum Geology Conference* (pp. 261–274). Geological Society.

Brewer, C. J., Hampson, G. J., Whittaker, A. C., Roberts, G. G., & Watkins, S. E. (2020). Comparison of methods to estimate sediment flux in ancient sediment routing systems. *Earth-Science Reviews*, *207*, 103217.

Brodie, J., & White, N. (1995). The link between sedimentary basin inversion and igneous underplating. In J. G. Buchanan & P. G. Buchanan (Eds.), *Basin inversion* (Vol. *88*, pp. 21–38). Geological Society, London, Special Publications.

Brown, S., & Richards, P. C. (1989). Facies and development of the middle Jurassic Brent Delta near the northern limit of its progradation, UK North Sea. In M. K. G. Whateley & K. T. Pickering (Eds.), *Deltas: Sites and traps for fossil fuels* (Vol. *41*, pp. 253–268). Geological Society, Special Publications.

Budding, M. C., & Inglin, H. F. (1981). A reservoir geological model of the Brent Sands in southern cormorant: Petroleum geology of the continental shelf of northwestern Europe. In V. Illing & G. D. Hobson (Eds.), *Petroleum geology of the continental shelf of north-west Europe* (pp. 326–334). Institute of Petroleum.

Bullimore, S. A., & Helland-Hansen, W. (2009). Trajectory analysis of the lower Brent Group (Jurassic), northern North Sea: Contrasting depositional patterns during the advance of a major deltaic system. *Basin Research*, *21*, 559–572.

Carroll, A. R., Chetel, L. M., & Smith, M. E. (2006). Feast to famine: Sediment supply control on Laramide Basin fill. *Geology*, *34*, 197–200.

Carvajal, C., & Steel, R. (2012). Source-to-sink sediment volumes within a tectono-stratigraphic model for a Laramide shelf-to-deep-water basin: Methods and results. In C. Busby & A. Azor (Eds.), *Tectonics of sedimentary basins: Recent advances* (pp. 131–151). Blackwell.

Chalmers, J. A., Green, P., Japsen, P., & Rasmussen, E. S. (2010). The Scandinavian mountains have not persisted since the Caledonian orogeny. A comment on Nielsen et al. (2009a). *Journal of Geodynamics*, *50*, 94–101.

Davies, S. J., Dawers, N. H., McLeod, A. E., & Underhill, J. R. (2000). The structural and sedimentological evolution of early synrift successions: The middle Jurassic Tarbert Formation, North Sea. *Basin Research*, *12*, 343–365.

Deegan, C. T., & Scull, B. J. (1977). A standard lithostratigraphic nomenclature for the central and northern North Sea. *Report of the Institute of Geological Sciences*, *77/25*, 1–35.

Deng, C., Fossen, H., Gawthorpe, R. L., Rotevatn, A., Jackson, C. A.-L., & Fazlikhani, H. (2017). Influence of fault reactivation during multiphase rifting: The Oseberg area, northern North Sea rift. *Marine and Petroleum Geology*, *86*, 1252–1272.

Dera, G., Brigaud, B., Monna, F., Laffont, R., Pucéat, E., Deconinck, J. F., Pellenard, P., Joachimski, M. M., & Durlet, C. (2011). Climatic ups and downs in a disturbed Jurassic world. *Geology*, *39*, 215–218.

Dickinson, W. R., & Gehrels, G. E. (2010). Insights into north American paleogeography and paleotectonics from U-Pb ages of detrital zircons in Mesozoic strata of the Colorado Plateau, USA. *International Journal of Earth Sciences*, *99*, 1247–1265.

Dromart, G., Garcia, J. P., Gaumet, F., Picard, S., Rousseau, M., Atrops, F., Lecuyer, C., & Sheppard, S. M. (2003). Perturbation of the carbon cycle at the middle/late Jurassic transition: Geological and geochemical evidence. *American Journal of Science*, *303*, 667–707.

Duffy, O. B., Bell, R. E., Jackson, C. A.-L., Gawthorpe, R. L., & Whipp, P. S. (2015). Fault growth and interactions in a multiphase rift fault network: Horda platform, Norwegian North Sea. *Journal of Structural Geology*, *80*, 99–119.

Duller, R. A., Armitage, J. J., Manners, H. R., Grimes, S., & Jones, T. D. (2019). Delayed sedimentary response to abrupt climate

change at the Paleocene-Eocene boundary, northern Spain. *Geology*, *47*, 159–162.

Duller, R. A., Whittaker, A. C., Fedele, J. J., Whitchurch, A. L., Springett, J., Smithells, R., Fordyce, S., & Allen, P. A. (2010). From grain size to tectonics. *Journal of Geophysical Research: Earth Surface*, *115*, F3.

Eide, C. H., Klausen, T. G., Katkov, D., Suslova, A. A., & Helland-Hansen, W. (2017). Linking an early Triassic delta to antecedent topography: Source-to-sink study of the southwestern Barents Sea margin. *Bulletin of the Geological Society of America*, *130*, 263–283.

Eide, C. H., Müller, R., & Helland-Hansen, W. (2018). Using climate to relate water discharge and area in modern and ancient catchments. *Sedimentology*, *65*, 1378–1389.

Eyal, H., Enzel, Y., Meiburg, E., Vowinckel, B., & Lensky, N. G. (2021). How does coastal gravel get sorted under stormy longshore transport? *Geophysical Research Letters*, *48*, e2021GL095082.

Færseth, R. B. (1996). Interaction of Permo-Triassic and Jurassic extensional fault-blocks during the development of the northern North Sea. *Journal of the Geological Society*, *153*, 931–944.

Fält, L. M., Helland, R., Jacobsen, V. W., & Renshaw, D. (1989). Correlation of transgressive-regressive depositional sequences in the middle Jurassic Brent/Vestland group megacycle, Viking Graben, Norwegian North Sea. In J. D. Collinson (Ed.), *Correlation in hydrocarbon exploration* (pp. 191–200). Graham and Trotman.

Fazlikhani, H., Fossen, H., Gawthorpe, R. L., Faleide, J. I., & Bell, R. E. (2017). Basement structure and its influence on the structural configuration of the northern North Sea rift. *Tectonics*, *36*, 1151–1177.

Fernandes, V. M., & Roberts, G. G. (2021). Cretaceous to recent net continental uplift from paleobiological data: Insights into subplate support. *Bulletin of the Geological Society of America*, *133*, 1217–1236.

Fjellanger, E., Olsen, T. R., & Rubino, J. L. (1996). Sequence stratigraphy and palaeogeography of the middle Jurassic Brent and Vestland deltaic systems, northern North Sea. *Norsk Geologisk Tidsskrift*, *76*, 75–106.

Flint, S., Knight, S., & Tilbrook, A. (1998). Application of high-resolution sequence stratigraphy to northwest Hutton field, northern North Sea: Implications for management of a mature Brent Group field. *AAPG Bulletin*, *82*, 1416–1436.

Folkestad, A., Odinsen, T., Fossen, H., & Pearce, M. A. (2014). Tectonic influence on the Jurassic sedimentary architecture in the northern North Sea with focus on the Brent Group. In A. W. Martinius, R. Ravnås, J. A. Howell, R. J. Steel, & J. P. Wonham (Eds.), *From depositional systems to sedimentary successions on the Norwegian continental margin* (Vol. *46*, pp. 389–416). International Association of Sedimentologists, Special Publications.

Ford, D., & Golonka, J. (2003). Phanerozoic paleogeography, paleoenvironment and lithofacies maps of the circum-Atlantic margins. *Marine and Petroleum Geology*, *20*, 249–285.

Friedrichs, C. T., & Wright, L. D. (2004). Gravity driven sediment transport on the continental shelf: Implications for equilibrium profiles near river mouths. *Coastal Engineering*, *51*, 795–811.

Gabrielsen, R. H., Faerseth, R. B., & Jensen, L. N. (1990). *Structural elements of the Norwegian continental shelf. Part 1: The Barents Sea region*. Norwegian Petroleum Directorate.

Gabrielsen, R. H., Faleide, J. I., Pascal, C., Braathen, A., Nystuen, J. P., Etzelmuller, B., & O'Donnell, S. (2010). Latest Caledonian to present tectonomorphological development of southern Norway. *Marine and Petroleum Geology*, *27*, 709–723.

Galloway, W. E. (1989). Genetic stratigraphic sequences in basin analysis I: architecture and genesis of flooding-surface bounded depositional units. *AAPG Bulletin*, *73*, 125–142.

Galloway, W. E., Whiteaker, T. L., & Ganey-Curry, P. (2011). History of Cenozoic north American drainage basin evolution, sediment yield, and accumulation in the Gulf of Mexico basin. *Geosphere*, *7*, 938–973.

Garzanti, E., Andò, S., & Vezzoli, G. (2009). Grain-size dependence of sediment composition and environmental bias in provenance studies. *Earth and Planetary Science Letters*, *277*, 422–432.

Ghadeer, S. G., & Macquaker, J. H. (2011). Sediment transport processes in an ancient mud-dominated succession: A comparison of processes operating in marine offshore settings and anoxic basinal environments. *Journal of the Geological Society*, *168*, 1121–1132.

Gilmullina, A., Klausen, T. G., Doré, A. G., Rossi, V. M., Suslova, A., & Eide, C. H. (2022). Linking sediment supply variations and tectonic evolution in deep time, source-to-sink systems—The Triassic Greater Barents Sea Basin. *GSA Bulletin*, *134*, 1760–1780.

Gomez-Veroiza, C. A., & Steel, R. J. (2017). Source to sink sandstone-mudstone proportion and facies distribution across a third-order clastic wedge, Cretaceous Western Interior Seaway. *Interpretation*, *5*, ST11–ST34.

Gong, C., Blum, M. D., Wang, Y., Lin, C., & Xu, Q. (2018). Can climatic signals be discerned in a deep-water sink? An answer from the Pearl River source-to-sink sediment-routing system. *Bulletin of the Geological Society of America*, *130*, 661–677.

Gradstein, F. M., Ogg, J. G., Schmitz, M. D., & Ogg, G. M. (Eds.). (2012). *The geologic time scale 2012*. Elsevier.

Graue, E., Helland-Hansen, W., Johnsen, J., Lømo, L., Nøttvedt, A., Rønning, K., Ryseth, A., & Steel, R. (1987). Advance and retreat of Brent delta system, Norwegian North Sea. In J. Brooks & K. Glennie (Eds.), *Petroleum geology of North West Europe* (Vol. *2*, pp. 915–937). Graham and Trotman.

Grimaud, J. L., Rouby, D., Chardon, D., & Beauvais, A. (2018). Cenozoic sediment budget ofWest Africa and The Niger delta. *Basin Research*, *30*, 169–186.

Guillocheau, F., Rouby, D., Robin, C., Helm, C., Rolland, N., De Veslud, C. L. C., & Braun, J. (2012). Quantification and causes of the terrigeneous sediment budget at the scale of a continental margin: A new method applied to the Namibia-South Africa margin. *Basin Research*, *24*, 3–30.

Hamilton, P. J., Fallick, A. E., Macintyre, R. M., & Elliot, S. (1987). Isotopic tracing of the provenance and diagenesis of lower Brent Group sands, North Sea. In J. Brooks & K. Glennie (Eds.), *Petroleum geology of North West Europe* (Vol. *2*, pp. 939–949). Graham and Trotman.

Hampson, G. J., Duller, R. A., Petter, A. L., Robinson, R. A. J., & Allen, P. A. (2014). Mass-balance constraints on stratigraphic interpretation of linked alluvial-coastal-shelfal deposits from source to sink: Example from Cretaceous Western Interior Basin, Utah and Colorado, USA. *Journal of Sedimentary Research*, *84*, 935–960.

Hampson, G. J., Sixsmith, P. J., & Johnson, H. D. (2004). A sedimentological approach to refining reservoir architecture in a mature hydrocarbon province: The Brent Province, UK North sea. *Marine and Petroleum Geology*, *21*, 457–484.

Haq, B. U. (2018). Jurassic Sea-level variations: A reappraisal. *GSA Today*, *28*, 4–10.

Harries, R. M., Kirstein, L. A., Whittaker, A. C., Attal, M., & Main, I. (2019). Impact of recycling and lateral sediment input on grain size fining trends—Implications for reconstructing tectonic and climate forcings in ancient sedimentary systems. *Basin Research*, *31*, 866–891.

Helland-Hansen, W., Ashton, M., Lømo, L., & Steel, R. (1992). Advance and retreat of the Brent delta: Recent contributions to the depositional model. In A. C. Morton, R. S. Haszeldine, M. R. Giles, & S. Brown (Eds.), *Geology of the Brent Group* (Vol. *61*, pp. 109–127). Geological Society, Special Publications.

Helland-Hansen, W., Sømme, T. O., Martinsen, O. J., Lunt, I., & Thurmond, J. (2016). Deciphering Earth's natural hourglasses: Perspectives on source-to-sink analysis. *Journal of Sedimentary Research*, *86*, 1008–1033.

Hessler, A. M., Zhang, J., Covault, J., & Ambrose, W. (2017). Continental weathering coupled to Paleogene climate changes in North America. *Geology*, *45*, 911–914.

Hinderer, M. (2012). From gullies to mountain belts: A review of sediment budgets at various scales. *Sedimentary Geology*, *280*, 21–59.

Hurst, A., & Morton, A. C. (1988). An application of heavy-mineral analysis to lithostratigraphy and reservoir modelling in the Oseberg Field, northern North Sea. *Marine and Petroleum Geology*, *5*, 157–169.

Husmo, T., Hamar, G. P., Høiland, O., Johannessen, E. P., Rømuld, A., Spencer, A. M., & Titterton, R. (2002). Lower and middle Jurassic. In D. Evans, C. Graham, A. Armour, & P. Bathurst (Eds.), *The millenium atlas: Petroleum geology of the central and northern North Sea* (pp. 129–155). Geological Society.

Japsen, P., Green, P. F., Nielsen, L. H., Rasmussen, E. S., & Bidstrup, T. (2007). Mesozoic–Cenozoic exhumation events in the eastern North Sea Basin: A multi-disciplinary study based on palaeothermal, palaeoburial, stratigraphic and seismic data. *Basin Research*, *19*, 451–490.

Jennette, D. C., & Riley, C. O. (1996). Influence of relative sea-level on facies and reservoir geometry of the middle Jurassic lower Brent Group, UK North Viking Graben. In J. A. Howell & J. F. Aitken (Eds.), *High resolution sequence stratigraphy: Innovations and application* (Vol. *104*, pp. 87–113). Geological Society, Special Publications.

Johannessen, E. R., Mjøs, R., Renshaw, D., Dalland, A., & Jacobsen, T. (1995). Northern limit of the "Brent delta" at the Tampen Spur—A sequence stratigraphic approach for sandstone prediction. In R. J. Steel, V. L. Felt, E. P. Johannessen, & C. Mathieu (Eds.), *Sequence stratigraphy on the northwest European margin* (Vol. *5*, pp. 213–256). Norwegian Petroleum Directorate, Special Publications.

Johannessen, K. C., Kohlmann, F., Ksienzyk, A. K., Dunkl, I., & Jacobs, J. (2013). Tectonic evolution of the SW Norwegian passive margin based on low-temperature thermochronology from the innermost Hardangerfjord area. *Norwegian Journal of Geology*, *93*, 243–260.

Ksienzyk, A. K., Dunkl, I., Jacobs, J., Fossen, H., & Kohlmann, F. (2014). From orogen to passive margin: Constraints from fission track and (U-Th)/He analyses on Mesozoic uplift and fault reactivation in SW Norway. In F. Corfu, D. Gasser, & D. M. Chew (Eds.), *New perspectives on the caledonides of scandinavia and related areas* (Vol. *390*, pp. 679–702). Geological Society, Special Publications.

Kuehl, S. A., Brunskill, G. J., Burns, K., Fugate, D., Kniskern, T., & Meneghini, L. (2004). Nature of sediment dispersal off the Sepik River, Papua New Guinea: Preliminary sediment budget and implications for margin processes. *Continental Shelf Research*, *24*, 2417–2429.

Latin, D. M. (1990). *The relationship between extension and magmatism in the North Sea Basin*. Unpublished PhD thesis. University of Edinburgh.

Latin, D. M., & Waters, F. G. (1992). Basaltic magmatism in the North Sea and its relationship to lithospheric extension. *Tectonophysics*, *208*, 77–90.

Li, Q., Gasparini, N. M., & Straub, K. M. (2018). Some signals are not the same as they appear: How do erosional landscapes transform tectonic history into sediment supply records? *Geology*, *46*, 407–410.

Lipp, A. G., Roberts, G. G., Whittaker, A. C., Gowing, C. J. B., & Fernandes, V. M. (2020). River sediment geochemistry as a conservative mixture of source regions: Observations and predictions from the Cairngorms, UK. *Journal of Geophysical Research: Earth Surface*, *125*, e2020JF005700.

Lipp, A. G., Roberts, G. G., Whittaker, A. C., Gowing, C. J. B., & Fernandes, V. M. (2021). Source region geochemistry from unmixing downstream sedimentary elemental compositions. *Geochemistry, Geophysics, Geosystems*, *22*, e2021GC009838-4634.

Liu, X., & Galloway, W. E. (1997). Quantitative determination of tertiary sediment supply to the North Sea Basin. *AAPG Bulletin*, *81*, 1482–1509.

Livera, S. E., & Caline, B. (1990). The sedimentology of the Brent Group in the Cormorant Block IV oilfield. *Journal of Petroleum Geology*, *13*, 367–396.

Lodhia, B. H., Roberts, G. G., Fraser, A. J., Jarvis, J., Newton, R., & Cowan, R. J. (2019). Observation and simulation of solid sedimentary flux: Examples from Northwest Africa. *Geochemistry, Geophysics, Geosystems*, *20*, 4613–4634.

Løseth, T. M., & Ryseth, A. (2003). A depositional and sequence stratigraphic model for the Rannoch and Etive formations, Oseberg Field, northern North Sea. *Norwegian Journal of Geology*, *83*, 87–106.

Lupker, M., Lavé, J., France-Lanord, C., Christl, M., Bourlès, D., Carcaillet, J., Maden, C., Wieler, R., Rahman, M., Bezbaruah, D., & Xiaohan, L. (2017). ^{10}Be systematics in the Tsangpo-Brahmaputra catchment: The cosmogenic nuclide legacy of the eastern Himalayan syntaxis. *Earth Surface Dynamics*, *5*, 429–449.

Lyster, S. J., Whittaker, A. C., Allison, P. A., Lunt, D. J., & Farnsworth, A. (2020). Predicting sediment discharges and erosion rates in deep time—Examples from the late cretaceous north American continent. *Basin Research*, *32*, 1547–1573.

Macquaker, J. H., Bentley, S. J., & Bohacs, K. M. (2010). Wave-enhanced sediment-gravity flows and mud dispersal across continental shelves: Reappraising sediment transport processes

operating in ancient mudstone successions. *Geology*, *38*, 947–950.

Manighetti, B., & Carter, L. (1999). Across-shelf sediment dispersal, Hauraki Gulf, New Zealand. *Marine Geology*, *160*, 271–300.

Martinsen, O. J., Sømme, T. O., Thurmond, J. B., Helland-Hansen, W., & Lunt, I. (2010). Source-to-sink systems on passive margins: Theory and practice with an example from the Norwegian continental margin. In B. A. Vining & S. C. Pickering (Eds.), *Petroleum geology: From mature basins to new frontiers—Proceedings of the 7th Petroleum Geology Conference* (pp. 913–920). Geological Society.

McKenzie, D., & O'Nions, R. K. (1991). Partial melt distributions from inversion of rare earth element concentrations. *Journal of Petrology*, *32*, 1021–1091.

McNab, F., Ball, P. W., Hoggard, M. J., & White, N. J. (2018). Neogene uplift and magmatism of Anatolia: Insights from drainage analysis and basaltic geochemistry. *Geochemistry, Geophysics, Geosystems*, *19*, 175–213.

Mearns, E. W. (1992). Samarium-neodymium isotopic constraints on the provenance of the Brent Group. In A. C. Morton, R. S. Haszeldine, M. R. Giles, & S. Brown (Eds.), *Geology of the Brent Group* (Vol. *61*, pp. 213–225). Geological Society, Special Publications.

Medvedev, S., & Hartz, E. H. (2015). Evolution of topography of post-Devonian Scandinavia: Effects and rates of erosion. *Geomorphology*, *231*, 229–245.

Michael, N. A., Whittaker, A. C., & Allen, P. A. (2013). The functioning of sediment routing systems using a mass balance approach: Example from the Eocene of the southern Pyrenees. *Journal of Geology*, *121*, 581–606.

Michael, N. A., Whittaker, A. C., Carter, A., & Allen, P. A. (2014). Volumetric budget and grain-size fractionation of a geological sediment routing system: Eocene Escanilla formation, south-central Pyrenees. *Bulletin of the Geological Society of America*, *126*, 585–599.

Milliman, J. D., & Farnsworth, K. L. (2011). *River discharge to the coastal ocean: A global synthesis*. Cambridge University Press.

Milliman, J. D., & Meade, R. H. (1983). World-wide delivery of river sediment to the oceans. *Journal of Geology*, *91*, 1–21.

Milliman, J. D., & Syvitski, J. P. M. (1992). Geomorphic/tectonic control of sediment discharge to the ocean: The importance of small mountainous rivers. *Journal of Geology*, *100*, 525–544.

Mitchener, B. C., Lawrence, D. A., Partington, M. A., Bowman, M. B. J., & Gluyas, J. (1992). Brent Group: Sequence stratigraphy and regional implications. In A. C. Morton, R. S. Haszeldine, M. R. Giles, & S. Brown (Eds.), *Geology of the Brent Group* (Vol. *61*, pp. 45–80). Geological Society, Special Publications.

Morris, J. E., Hampson, G. J., & Maxwell, G. (2003). Controls on facies architecture in the Brent Group, Strathspey Field, UK North sea: Implications for reservoir characterization. *Petroleum Geoscience*, *9*, 209–220.

Morton, A., Hallsworth, C., Strogen, D., Whitham, A., & Fanning, M. (2009). Evolution of provenance in the NE Atlantic rift: The early–middle Jurassic succession in the Heidrun field, Halten terrace, offshore mid-Norway. *Marine and Petroleum Geology*, *26*, 1100–1117.

Morton, A. C. (1985). A new approach to provenance studies: Electron microprobe analysis of detrital garnets from middle Jurassic sandstones of the northern North Sea. *Sedimentology*, *32*, 553–566.

Morton, A. C. (1992). Provenance of Brent Group sandstones: Heavy mineral constraints. In A. C. Morton, R. S. Haszeldine, M. R. Giles, & S. Brown (Eds.), *Geology of the Brent Group* (Vol. *61*, pp. 227–244). Geological Society, Special Publications.

Morton, A. C., Hallsworth, C., & Chalton, B. (2004). Garnet compositions in Scottish and Norwegian basement terrains: A framework for interpretation of North Sea sandstone provenance. *Marine and Petroleum Geology*, *21*, 393–410.

Mulder, T., Syvitski, J. P., Migeon, S., Faugères, J. C., & Savoye, B. (2003). Marine hyperpycnal flows: Initiation, behavior and related deposits. A review. *Marine and Petroleum Geology*, *20*, 861–882.

Nielsen, S. B., Gallagher, K., Leighton, C., Balling, N., Svenningsen, L., Jacobsen, B. H., Thomsen, E., Nielsen, O. B., Heilmann-Clausen, C., Egholm, D. L., Summerfield, M. A., Clausen, O. R., Piotrowski, J. A., Thorsen, M. R., Huuse, M., Abrahamsen, N., King, C., & Lykke-Andersen, H. (2009). The evolution of western Scandinavian topography: A review of Neogene uplift versus the ICE (isostasy-climate-erosion) hypothesis. *Journal of Geodynamics*, *47*, 72–95.

Nirrengarten, M., Gernigon, L., & Manatschal, G. (2014). Lower crustal bodies in the Møre volcanic rifted margin: Geophysical determination and geological implications. *Tectonophysics*, *636*, 143–157.

Nyberg, B., Helland-Hansen, W., Gawthorpe, R. L., Tillmans, F., & Sandbakken, P. (2021). Assessing first-order BQART estimates for ancient source-to-sink mass budget calculations. *Basin Research*, *33*, 2435–2452.

Ogg, J. G., Ogg, G. M., & Gradstein, F. M. (2016). *A concise geologic time scale*. Elsevier.

Paola, C., Ganti, V., Mohrig, D., Runkel, A. C., & Straub, K. M. (2018). Time not our time: Physical controls on the preservation and measurement of geologic time. *Annual Review of Earth and Planetary Sciences*, *46*, 409–438.

Paola, C., & Martin, J. M. (2012). Mass-balance effects in depositional systems. *Journal of Sedimentary Research*, *82*, 435–450.

Parsons, A. J., Michael, N. A., Whittaker, A. C., Duller, R. A., & Allen, P. A. (2012). Grain-size trends reveal the late orogenic tectonic and erosional history of the south-central Pyrenees, Spain. *Journal of the Geological Society*, *169*, 111–114.

Partington, M. A., Copestake, P., Mitchener, B. C., & Underhill, J. R. (1993). Biostratigraphic calibration of genetic stratigraphic sequences in the Jurassic–lowermost cretaceous (Hettangian to Ryazanian) of the North Sea and adjacent areas. In J. R. Parker (Ed.), *Petroleum geology of Northwest Europe: Proceedings of the 4th Petroleum Geology Conference* (pp. 371–386). Geological Society.

Petter, A. L., Steel, R. J., Mohrig, D., Kim, W., & Carvajal, C. (2013). Estimation of the paleoflux of terrestrial-derived solids across ancient basin margins using the stratigraphic record. *Bulletin of the Geological Society of America*, *125*, 578–593.

Phillips, T. B., Fazlikhani, H., Gawthorpe, R. L., Fossen, H., Jackson, C. A.-L., Bell, R. E., Faleide, J. I., & Rotevatn, A. (2019). The influence of structural inheritance and multiphase extension on rift development, the northern North Sea. *Tectonics*, *38*, 4099–4126.

Plank, T., & Forsyth, D. W. (2016). Thermal structure and melting conditions in the mantle beneath the basin and range province from seismology and petrology. *Geochemistry, Geophysics, Geosystems*, *17*, 1312–1338.

Plint, A. G. (2014). Mud dispersal across a cretaceous prodelta: Storm-generated, wave-enhanced sediment gravity flows inferred from mudstone microtexture and microfacies. *Sedimentology*, *61*, 609–647.

Pratt-Sitaula, B., Garde, M., Burbank, D. W., Oskin, M., Heimsath, A., & Gabet, E. (2007). Bedload-to-suspended load ratio and rapid bedrock incision from Himalayan landslide-dam lake record. *Quaternary Research*, *68*, 111–120.

Prokoph, A., Shields, G. A., & Veizer, J. (2008). Compilation and time-series analysis of a marine carbonate $\delta^{18}O$, $\delta^{13}C$, $^{87}Sr/^{86}Sr$ and $\delta^{34}S$ database through earth history. *Earth-Science Reviews*, *87*, 113–133.

Quirie, A. K., Schofield, N., Hartley, A., Hole, M. J., Archer, S. G., Underhill, J. R., Watson, D., & Holford, S. P. (2019). The Rattray Volcanics: Mid-Jurassic fissure volcanism in the UK Central North Sea. *Journal of the Geological Society*, *176*, 462–481.

Quirie, A. K., Schofield, N., Jolley, D. W., Archer, S. G., Hole, M. J., Hartley, A., Watson, D., Burgess, R., Pugsley, J. H., Underhill, J. R., & Holford, S. P. (2020). Palaeogeographical evolution of the Rattray Volcanic Province, Central North Sea. *Journal of the Geological Society*, *177*, 718–737.

Rattey, R. P., & Hayward, A. B. (1993). Sequence stratigraphy of a failed rift system: The middle Jurassic to early cretaceous basin evolution of the central and northern North Sea. In J. R. Parker (Ed.), *Petroleum geology of Northwest Europe: Proceedings of the 4th Petroleum Geology Conference* (pp. 215–249). Geological Society.

Ravnås, R., Nøttvedt, A., Steel, R. J., & Windelstad, J. (2000). Syn-rift sedimentary architectures in the northern North Sea. In A. Nøttvedt (Ed.), *Sequence stratigraphy on the northwest European margin* (Vol. *167*, pp. 133–177). Geological Society, Special Publications.

Reynolds, A. D. (1995). Sedimentology and sequence stratigraphy of the thistle field, northern North Sea. In R. J. Steel, V. L. Felt, E. P. Johannessen, & C. Mathieu (Eds.), *Sequence stratigraphy on the northwest European margin* (Vol. *5*, pp. 257–271). Norwegian Petroleum Directorate, Special Publications.

Reynolds, A. D. (2019). "Grain-size bookkeeping", a new aid for siliciclastic systems with examples from paralic environments. *Journal of Sedimentary Research*, *89*, 976–1016.

Rohais, S., & Rouby, D. (2020). Source-to-sink analysis of the Plio-Pleistocene deposits in the Suez rift (Egypt). In S. Khomsi, F. Roure, M. Al Garni, & A. Amin (Eds.), *Arabian plate and surroundings: Geology, sedimentary basins and georesources* (pp. 115–133). Springer.

Romans, B. W., Castelltort, S., Covault, J. A., Fildani, A., & Walsh, J. P. (2016). Environmental signal propagation in sedimentary systems across timescales. *Earth-Science Reviews*, *153*, 7–29.

Rowley, D. B. (2007). Stable isotope-based paleoaltimetry: Theory and validation. *Reviews in Mineralogy and Geochemistry*, *66*, 23–52.

Sadler, P. M. (1981). Sediment accumulation rates and the completeness of stratigraphic sections. *Journal of Geology*, *89*, 569–584.

Sadler, P. M. (1999). The influence of hiatuses on sediment accumulation rates. *GeoResearch Forum*, *5*, 15–40.

Schudack, M. E. (1999). Ostracoda (marine/nonmarine) and palaeoclimate history in the upper Jurassic of Central Europe and North America. *Marine Micropaleontology*, *37*, 273–288.

Sclater, J. G., & Christie, P. A. (1980). Continental stretching: An explanation of the post-mid-cretaceous subsidence of the central North Sea Basin. *Journal of Geophysical Research: Solid Earth*, *85*, 3711–3739.

Sellwood, B. W., & Valdes, P. J. (2006). Mesozoic climates: General circulation models and the rock record. *Sedimentary Geology*, *190*, 269–287.

Sellwood, B. W., & Valdes, P. J. (2008). Jurassic climates. *Proceedings of the Geologists Association*, *119*, 5–17.

Sharman, G. R., Covault, J. A., Stockli, D. F., Wroblewski, A. F. J., & Bush, M. A. (2017). Early Cenozoic drainage reorganization of the United States Western Interior–Gulf of Mexico sediment routing system. *Geology*, *45*, 187–190.

Sharman, G. R., & Johnstone, S. A. (2017). Sediment unmixing using detrital geochronology. *Earth and Planetary Science Letters*, *477*, 183–194.

Sharman, G. R., Sylvester, Z., & Covault, J. A. (2019). Conversion of tectonic and climatic forcings into records of sediment supply and provenance. *Scientific Reports*, *9*, 1–7.

Shorttle, O., Maclennan, J., & Lambart, S. (2014). Quantifying lithological variability in the mantle. *Earth and Planetary Science Letters*, *395*, 24–40.

Simon Petroleum Technology Ltd. (1994). *The Brent Delta—An integrated sedimentological and palynological study of the Brent Group between latitudes 59^0N and 62^0N, UK and Norwegian sectors, North Sea*. Unpublished Report for Shell UK Expro.

Skarpnes, O., Hamar, G. P., Jakobsson, K. H., & Ormaasen, D. E. (1980). Regional Jurassic setting of the North Sea north of the central highs. In *Proceedings of symposium "the sedimentation of the North Sea reservoir rocks"* (Paper XIII, pp. 1–8). Norwegian Petroleum Society.

Slater, S. M., McKie, T., Vieira, M., Wellman, C. H., & Vajda, V. (2017). Episodic river flooding events revealed by palynological assemblages in Jurassic deposits of the Brent Group, North Sea. *Palaeogeography, Palaeoclimatology, Palaeoecology*, *485*, 389–400.

Smelror, M., Dehls, J., Ebbing, J., Larsen, E., Lundin, E. R., Nordgulen, Ø., Osmundsen, P. T., Olesen, O., Ottesen, D., Pascal, C., & Redfield, T. F. (2007). Towards a 4D topographic view of the Norwegian Sea margin. *Global and Planetary Change*, *58*, 382–410.

Sneider, J. S., de Clarens, P., & Vail, P. R. (1995). Sequence stratigraphy of the middle to upper Jurassic, Viking Graben, North Sea. In R. J. Steel, V. L. Felt, E. P. Johannessen, & C. Mathieu (Eds.), *Sequence stratigraphy on the northwest European margin* (Vol. *5*, pp. 167–197). Norwegian Petroleum Directorate, Special Publications.

Sømme, T. O., Helland-Hansen, W., Martinsen, O. J., & Thurmond, J. B. (2009). Relationships between morphological and sedimentological parameters in source-to-sink systems: A basis for predicting semi-quantitative characteristics in subsurface systems. *Basin Research*, *21*, 361–387.

Sømme, T. O., & Jackson, C. A.-L. (2013). Source-to-sink analysis of ancient sedimentary systems using a subsurface case study from the Møre-Trøndelag area of southern Norway: Part 2—Sediment dispersal and forcing mechanisms. *Basin Research*, *25*, 512–531.

Sømme, T. O., Martinsen, O. J., & Lunt, I. (2013). Linking offshore stratigraphy to onshore paleotopography: The late Jurassic-Paleocene evolution of the south Norwegian margin. *Bulletin of the Geological Society of America*, *125*, 1164–1186.

Steel, R. J. (1993). Triassic-Jurassic megasequence stratigraphy in the northern North Sea: Rift to post-rift evolution. In J. R. Parker (Ed.), *Petroleum geology of Northwest Europe: Proceedings of the 4th Petroleum Geology Conference* (pp. 299–315). Geological Society.

Steel, R. J., & Ryseth, A. (1990). The Triassic – Early Jurassic succession in the northern North Sea: Megasequence stratigraphy and intra-Triassic tectonics. In R. P. F. Hardman & J. Brooks (Eds.), *Tectonic events responsible for Britain's oil and gas reserves* (Vol. *55*, pp. 139–168). Geological Society, Special Publications.

Sun, B., Wang, Y. F., Li, C. S., Yang, J., Li, J. F., Li, Y. L., Deng, T., Wang, S. Q., Zhao, M., Spicer, R. A., & Ferguson, D. K. (2015). Early Miocene elevation in northern Tibet estimated by palaeobotanical evidence. *Scientific Reports*, *5*, 1–6.

Syvitski, J. P. M., & Milliman, J. D. (2007). Geology, geography, and humans battle for dominance over the delivery of fluvial sediment to the coastal ocean. *Journal of Geology*, *115*, 1–19.

Syvitski, J. P. M., Peckham, S. D., Hilberman, R., & Mulder, T. (2003). Predicting the terrestrial flux of sediment to the global ocean: A planetary perspective. *Sedimentary Geology*, *162*, 5–24.

Tappe, S., Smart, K. A., Stracke, A., Romer, R. L., Prelević, D., & van den Bogaard, P. (2016). Melt evolution beneath a rifted craton edge: $^{40}Ar/^{39}Ar$ geochronology and Sr–Nd–Hf–Pb isotope systematics of primitive alkaline basalts and lamprophyres from the SW Baltic shield. *Geochimica et Cosmochimica Acta*, *173*, 1–36.

Tinker, J. M., de Wit, M., & Brown, R. (2008). Mesozoic exhumation of the southern cape, South Africa, quantified using apatite fission track thermochronology. *Tectonophysics*, *455*, 77–93.

Torsvik, T. H., Carlos, D., Mosar, J., Cocks, L. R. M., & Malme, T. (2002). Global reconstructions and North Atlantic paleogeography 440 Ma to recent. In E. Eide (Ed.), *BATLAS—Mid Norway plate reconstruction atlas with global and Atlantic perspectives* (pp. 18–39). Geological Survey of Norway.

Traykovski, P., Wiberg, P. L., & Geyer, W. R. (2007). Observations and modeling of wave-supported sediment gravity flows on the Po prodelta and comparison to prior observations from the eel shelf. *Continental Shelf Research*, *27*, 375–399.

Turowski, J. M., Rickenmann, D., & Dadson, S. J. (2010). The partitioning of the total sediment load of a river into suspended load and bedload: A review of empirical data. *Sedimentology*, *57*, 1126–1146.

Underhill, J. R. (1998). Jurassic. In K. W. Glennie (Ed.), *Petroleum geology of the North Sea: Basic concepts and recent advances* (4th ed., pp. 245–292). Blackwell.

Underhill, J. R., & Partington, M. A. (1993). Jurassic thermal doming and deflation in the North Sea: Implications of the sequence stratigraphic evidence. In J. R. Parker (Ed.), *Petroleum geology of Northwest Europe: Proceedings of the 4th Petroleum Geology Conference* (pp. 337–345). Geological Society.

Underhill, J. R., & Partington, M. A. (1994). Use of genetic sequence stratigraphy in defining and determining a regional tectonic control on the "mid cimmerian unconformity": Implications for North Sea Basin development and the global sea-level chart. In P. Weimer & H. W. Posamentier (Eds.), *Siliciclastic sequence stratigraphy: Recent developments and applications* (Vol. *58*, pp. 449–484). AAPG, Memoirs.

Walford, H. L., White, N. J., & Sydow, J. C. (2005). Solid sediment load history of the Zambezi Delta. *Earth and Planetary Science Letters*, *238*, 49–63.

Walsh, J. P., & Nittrouer, C. A. (2003). Contrasting styles of off-shelf sediment accumulation in New Guinea. *Marine Geology*, *196*, 105–125.

Wapenhans, I., Fernandes, V. M., O'Malley, C., White, N., & Roberts, G. G. (2021). Scale-dependent contributors to river profile geometry. *Journal of Geophysical Research: Earth Surface*, *126*, e2020JF005879.

Watkins, S. E., Whittaker, A. C., Bell, R. E., Brooke, S. A., Ganti, V., Gawthorpe, R. L., McNeill, L. C., & Nixon, C. W. (2020). Straight from the source's mouth: Controls on field-constrained sediment export across the entire active Corinth Rift, Central Greece. *Basin Research*, *32*, 1600–1625.

Watkins, S. E., Whittaker, A. C., Bell, R. E., McNeill, L. C., Gawthorpe, R. L., Brooke, S. A., & Nixon, C. W. (2018). Are landscapes buffered to high-frequency climate change? A comparison of sediment fluxes and depositional volumes in the Corinth Rift, Central Greece, over the past 130 ky. *Bulletin of the Geological Society of America*, *131*, 372–388.

Weltje, G. J., & Brommer, M. B. (2011). Sediment-budget modelling of multi-sourced basin fills: Application to recent deposits of the western Adriatic mud wedge (Italy). *Basin Research*, *23*, 291–308.

Whitaker, M. F., Giles, M. R., & Cannon, S. J. C. (1992). Palynological review of the Brent Group, UK sector, North Sea. In A. C. Morton, R. S. Haszeldine, M. R. Giles, & S. Brown (Eds.), *Geology of the Brent Group* (Vol. *61*, pp. 169–202). Geological Society, Special Publications.

Whitchurch, A. L., Carter, A., Sinclair, H. D., Duller, R. A., Whittaker, A. C., & Allen, P. A. (2011). Sediment routing system evolution within a diachronously uplifting orogen: Insights from detrital zircon thermochronological analyses from the South-Central Pyrenees. *American Journal of Science*, *311*, 442–482.

White, N. (1989). Nature of lithospheric extension in the North Sea. *Geology*, *17*, 111–114.

Whittaker, A. C., Attal, M., & Allen, P. A. (2010). Characterising the origin, nature and fate of sediment exported from catchments perturbed by active tectonics. *Basin Research*, *22*, 809–828.

Whittaker, A. C., Duller, R. A., Springett, J., Smithells, R. A., Whitchurch, A. L., & Allen, P. A. (2011). Decoding downstream trends in stratigraphic grain size as a function of tectonic subsidence and sediment supply. *Bulletin of the Geological Society of America*, *123*, 1363–1382.

Zanella, E., & Coward, M. P. (2003). Structural framework. In D. Evans, C. Graham, A. Armour, & P. Bathurst (Eds.), *The millenium atlas: Petroleum geology of the central and northern North Sea* (pp. 45–59). Geological Society.

Zhang, J., Covault, J., Pyrcz, M., Sharman, G. R., Carvajal, C., & Milliken, K. (2018). Quantifying sediment supply to continental margins: Application to the Paleogene Wilcox Group, Gulf of Mexico. *AAPG Bulletin*, *102*, 1685–1702.

Ziegler, P. A. (1990). Tectonic and palaeogeographic development of the North Sea rift system. In D. J. Blundell & A. D. Gibbs (Eds.), *Tectonic evolution of the North Sea rifts* (pp. 1–36). Oxford University Press.

Zondervan, J. R., Whittaker, A. C., Bell, R. E., Watkins, S. E., Brooke, S. A., & Hann, M. G. (2020). New constraints on bedrock erodibility and landscape response times upstream of an active fault. *Geomorphology*, *351*, 106937.

SUPPORTING INFORMATION

Additional supporting information can be found online in the Supporting Information section at the end of this article.

How to cite this article: Okwara, I. C., Hampson, G. J., Whittaker, A. C., Roberts, G. G., & Ball, P. W. (2023). Source-to-sink mass-balance analysis of an ancient wave-influenced sediment routing system: Middle Jurassic Brent Delta, Northern North Sea, offshore UK and Norway. *Basin Research*, *00*, 1–35. https://doi.org/10.1111/bre.12765